J|A|C|S
ARTICLES
Published on Web 10/04/2006

Reorganization Free Energies for Long-Range Electron Transfer in a Porphyrin-Binding Four-Helix Bundle Protein

Jochen Blumberger* and Michael L. Klein

Contribution from the Center for Molecular Modeling and Department of Chemistry, University of Pennsylvania, 231 South 34th Street, Philadelphia, Pennsylvania 19104-6323

Received June 9, 2006; E-mail: jochen@cmm.upenn.edu

Abstract: To explore the possibility of electron transport in a recently designed four-helix bundle protein (Cochran, F. V.; et al. *J. Am. Chem. Soc.* **2005**, *127*, 1346), we have computed the reorganization free energy for (i) oxidation of a single Ru−porphyrin cofactor and (ii) electron self-exchange between two Ru−porphyrin cofactors binding to the solvated protein. Sampling the classical electrostatic energy gap for 20 ns, we find that the fluctuations are well described by Gaussian statistics and obtain reorganization free energies of 0.90 ± 0.04 eV for oxidation and 1.36 ± 0.08 eV for self-exchange. The latter is 0.1−0.2 eV higher than the experimental estimate for interprotein electron self-exchange in cytochrome b5. As in natural electron carriers, inner-sphere reorganization is very small, 88 meV for self-exchange between two model cofactors computed at the density functional level of theory. Decomposing the outer-sphere reorganization free energy, we find that the solvent (aqueous ionic solution) is the primary outer-sphere medium for oxidation, contributing 0.60 eV (69%). The protein contributes only 0.27 eV (31%). For self-exchange, the solvent contribution, 0.68 eV (54%), and the protein contribution, 0.59 eV (46%), are almost equally important. The large solvent contribution is due to the slow decay of dipole reorientation of the solvent as a function of distance to the cofactor, implying that the change in the electric field upon electron transfer is not as effectively screened by the four-helix bundle protein. However, ranking the residues according to their free energy contributions, it is suggested that the reorganization free energy can be decreased by about 0.2 eV if two glutamine residues in the vicinity of the cofactor are mutated into less polar amino acids.

1. Introduction

In recent years, it has become possible to design simple and stable polypeptides that accommodate functional elements of natural proteins.[1−8] Redox-active nanoscale materials such as porphyrin binding proteins are of immense interest because of their potential use as bioelectronic devices or as catalysts in light-energy harvesting processes coupled to hydrogen and oxygen production. Because of their simple structure and stability and the relative ease with which they can be mutated, designed redox proteins also offer the possibility of systematic study of the various factors that govern the rate of biological electron-transfer (ET) reactions.[9−11] In the present study we investigate one of these factors, the reorganization free energy for long-range electron transfer in a recently designed four-helix bundle protein[2] (see Figure 1).

In the Marcus picture of non-adiabatic electron transfer, the rate is determined by three key quantities:[12,13] reorganization free energy, λ; redox potential difference of the two cofactors or free energy difference, ΔA; and electronic coupling between donor and acceptor, H_{12}.

$$k_{\mathrm{ET}} = \sqrt{\frac{4\pi^3}{h^2\lambda RT}}{H_{12}}^2 \exp\left(-\frac{(\Delta A + \lambda)^2}{4\lambda RT}\right) \qquad (1)$$

The exponential in eq 1 implies that a suitable balance between λ and ΔA is crucial for efficient electron transfer, which is predicted to have a maximum rate for $\lambda = -\Delta A$. Redox potentials of natural and synthetic porphyrins range from −0.4 to 0.4 V relative to standard hydrogen electrode, implying that λ should be close to or smaller than 1 eV for efficient thermal ET between two porphyrin cofactors. This criterion is indeed met by most natural porphyrin-based electron carriers[11,14] and should be compared to the large reorganization free energy for self-exchange ($\Delta A = 0$) between ferrous and ferric aqua ions, ∼2.1 eV.[15,16]

(1) Chen, X.; Discher, B. M.; Pilloud, D. L.; Gibney, B. R.; Moser, C. C.; Dutton, P. L. *J. Phys. Chem. B* **2002**, *106*, 617.
(2) Cochran, F. V.; Wu, S. P.; Wang, W.; Nanda, V.; Saven, J. G.; Therien, M. J.; DeGrado, W. F. *J. Am. Chem. Soc.* **2005**, *127*, 1346.
(3) Nanda, V.; Rosenblatt, M. M.; Osyczka, A.; Kono, H.; Getahun, Z.; Dutton, P. L.; Saven, J. G.; DeGrado, W. F. *J. Am. Chem. Soc.* **2005**, *127*, 5804.
(4) Noy, D.; Discher, B. M.; Rubtsov, I. V.; Hochstrasser, R. A.; Dutton, P. L. *Biochemistry* **2005**, *44*, 12344.
(5) Ye, S. X.; Discher, B. M.; Strzalka, J.; Xu, T.; Wu, S. P.; Noy, D.; Kuzmenko, I.; Gog, T.; Therien, M. J.; Dutton, P. L.; Blasie, J. K. *Nano Lett.* **2005**, *5*, 1658.
(6) Lu, Y. *Curr. Opin. Struct. Biol.* **2005**, *9*, 118.
(7) Fairman, R.; Akerfeldt, K. S. *Curr. Opin. Struct. Biol.* **2005**, *15*, 453.
(8) Kovaric, B. C.; Kokona, B.; Schwab, A. D.; Twomey, M. A.; de Paula, J. C.; Fairman, R. *J. Am. Chem. Soc.* **2006**, *128*, 4166.
(9) Marcus, R. A.; Sutin, N. *Biochim. Biophys. Acta* **1985**, *811*, 265.
(10) Moser, C. C.; Keske, J. M.; Warncke, K.; Farid, R. S.; Dutton, P. L. *Nature* **1992**, *355*, 796.
(11) Gray, H. B.; Winkler, J. R. *Q. Rev. Biophys.* **2003**, *36*, 341.
(12) Marcus, R. A. *J. Chem. Phys.* **1956**, *24*, 966.
(13) Marcus, R. A. *J. Chem. Phys.* **1965**, *43*, 679.
(14) Simonneaux, G.; Bondon, A. *Chem. Rev.* **2005**, *105*, 2627.
(15) Rosso, K. M.; Rustad, J. R. *J. Phys. Chem. A* **2000**, *104*, 6718.
(16) Sit, P. H.-L.; Cococcioni, M.; Marzari, N. *Phys. Rev. Lett.* **2006**, *97*, 028303.

10.1021/ja063852t CCC: $33.50

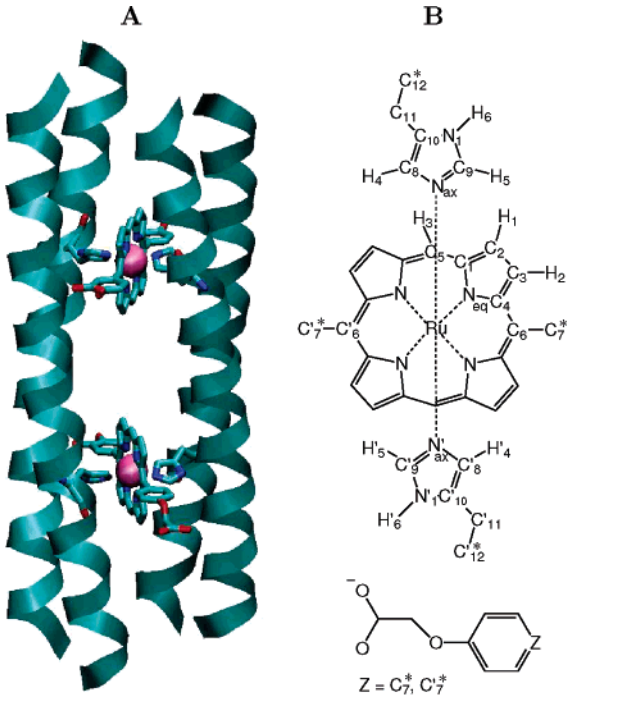

C LEEAL QEAQQ TAQEA QQALQ KHQQA FQKFQ KY

D
LEU1 ····· HIS22 ····· TYR32
TYR96 ····· HIS86 ····· LEU65
POR2 POR1
TYR128 ····· HIS118 ····· LEU97
LEU33 ····· HIS54 ····· TYR64

Figure 1. (A) Model structure of the simulated four-helix bundle protein binding two RuDPP cofactors.[2] The protein is comprised of two antiparallel pairs of α-helices (shown in ribbon representation) and is D_2 symmetric. The helices are sequence identical, each helix is composed of 32 amino acids. The two RuDPP cofactors, POR1 and POR2, and the axial histidine ligands, HIS22, HIS54 and HIS86, HIS118, are depicted in stick representation. Color code: C, green; N, blue; O, red. The Ru atom is depicted as a purple sphere, and hydrogen atoms are removed. (B) Structure and atom definition for the RuDPP cofactor and axial histidine ligands. All atoms in the upper part of panel B are treated as QM atoms in QM/MM molecular dynamics simulations and are treated as ionizable atoms in classical molecular dynamics simulations. Atoms at the QM/MM boundary are labeled with an asterisk (*) and described with monovalent pseudopotentials. The aryl rest (lower part of panel B) that is covalently attached to the porphin ring in the C_6 and C_6' positions is treated with a classical force field in QM/MM simulations. (C) Amino acid sequence of a helix. (D) Scheme of amino acid sequence for the four-helix bundle.

The small reorganization free energy in natural porphyrin-based electron carriers, 0.5−1.2 eV, is accomplished with little structural change[17,18] of cofactor and ligands ("inner-sphere") upon oxidation. Very recently, Gray and co-workers reported a value of 120−140 meV for the reorganization energy of Zn−porphyrins obtained from gas-phase photoelectron spectroscopy.[19] Also, ab initio calculations have predicted small reorganization energies for Fe−porphins ligated to histidine and methionine ligands, 50−85 meV.[18] A second mechanism by which proteins reduce reorganization free energy is spatial separation of donor and acceptor from the solvent. The redox-active cofactors are usually buried in the hydrophobic interior of the protein, which is far less susceptible to a change in charge than water and the polar residues at the surface of the protein.

The very small inner-sphere reorganization of porphyrin cofactors suggests that the dominant contribution to the total reorganization free energy comes from protein and solvent ("outer-sphere"). Although most relevant for efficient ET, the protein and solvent contributions to ET are not well understood. This is probably related to the difficulty of describing the inherently inhomogeneous protein matrix with continuum models[20−22] and due to the fact that most experimental techniques yield the sum of outer-sphere contributions, not distinguishing between the effects of protein and solvent. An exception are measurements for hemoglobin hybrids in cryogenic glasses which suggested that the polypeptide is the primary outer-sphere medium and that reorganization of the bulk solvent is less important.[23] Given the high significance of outer-sphere reorganization for electron transfer in native and designed proteins, it is clearly desirable to understand its origin and decomposition in more detail.

While redox potentials of cofactors bound to proteins can be measured to high precision (see, e.g., references in ref 24), the reorganization free energy is not an experimental observable and has to be determined indirectly and often with rather large uncertainties by fitting experimental data to the rate expression of Marcus. In this regard, computer simulations are a valuable alternative for quantitative estimation of reorganization free energies. Moreover, the validity of the linear response assumption leading to parabolic free energy curves in Marcus theory does not have to be asserted but can be assessed using force field-based[22,25,26] or, better, ab initio molecular dynamics (MD)[16,27−29] combined with enhanced sampling methods. Simonson showed that the fluctuations in yeast cytochrome *c* (cyt c) have indeed a Gaussian form and reported a reorganization free energy for oxidation in reasonably good agreement with experiment, $\lambda = 0.77$ eV,[26] compared to 0.61 ± 0.03 eV obtained from ET measurements.[30] Earlier MD simulations of self-exchange between two cyt c's by Warshel and co-workers[22] also gave fair agreement with experiment, even though the modeling of the encounter complex was done in a less rigorous way.

Using quantum mechanical calculations, mixed quantum-classical (QM/MM), and classical molecular dynamics simulation, we investigate herein inner- and outer-sphere reorganization free energy for (i) oxidation of a porphyrin cofactor and (ii) electron transfer between two porphyrin cofactors binding to the four-helix bundle (see Figure 1). The solvent and protein contributions of the outer-sphere reorganization are calculated, allowing us to identify the residues that contribute most to the reorganization free energy. Anticipating our results, we find that the electrostatic energy gap fluctuations of the four-helix bundle are well described in the linear response approximation that underlies Marcus theory. While inner-sphere reorganization for

(17) Takano, T.; Dickerson, R. E. *J. Mol. Biol.* **1981**, *153*, 95.
(18) Sigfridsson, E.; Olsson, M.; Ryde, U. *J. Phys. Chem. B* **2001**, *105*, 5546.
(19) Amashukeli, X.; Gruhn, N. E.; Lichtenberger, D. L.; Winkler, J. R.; Gray, H. B. *J. Am. Chem. Soc.* **2004**, *126*, 15566.
(20) Zhou, H.-X. *J. Am. Chem. Soc.* **1994**, *116*, 10362.
(21) Basu, G.; Kitao, A.; Kuki, A.; Go, N. *J. Phys. Chem. B* **1998**, *102*, 2076.
(22) Muegge, I.; Qi, P. X.; Wand, A. J.; Chu, Z. T.; Warshel, A. *J. Phys. Chem. B* **1997**, *101*, 825.
(23) Kuila, D.; Baxter, W. W.; Natan, M. J.; Hoffman, B. M. *J. Phys. Chem. B* **1991**, *95*, 1.
(24) Mao, J.; Hauser, K.; Gunner, M. R. *Biochemistry* **2003**, *42*, 9829.
(25) Sterpone, F.; Ceccarelli, M.; Marchi, M. *J. Phys. Chem. B* **2003**, *107*, 11208.
(26) Simonson, T. *Proc. Natl. Acad. Sci. U.S.A.* **2002**, *99*, 6544.
(27) Blumberger, J.; Tavernelli, I.; Klein, M. L.; Sprik, M. *J. Chem. Phys.* **2006**, *124*, 64507.
(28) Blumberger, J.; Sprik, M. *Theor. Chem. Acc.* **2006**, *115*, 113.
(29) Blumberger, J.; Sprik, M. *J. Phys. Chem. B* **2005**, *109*, 6793.
(30) Terrettaz, S.; Cheng, J.; Miller, C. J.; Guiles, R. D. *J. Am. Chem. Soc.* **1996**, *118*, 7857.

electron self-exchange is similarly small as in natural cofactors, about 0.1 eV, the outer-sphere reorganization free energy is large, 1.2−1.3 eV. Approximately half of the outer-sphere contribution is due to the solvent, and half of it is due to the protein. We suggest that the outer-sphere contribution could be lowered by mutation of two dipolar glutamine residues in the vicinity of the cofactor.

This paper is organized as follows. In section 2, we review the formulas used to compute diabatic free energy curves for ET and give details on gas-phase calculations and QM/MM and classical molecular dynamics simulation. In section 3, results on structure, ligation, and inner-sphere reorganization of model cofactors in the gas phase and of the full cofactor in the protein (QM/MM) are presented. Protein dynamics, solvation, and root-mean-square deviations obtained from long classical molecular dynamics simulation are discussed for both oxidation states. We then present diabatic free energy profiles for oxidation and electron self-exchange obtained from classical molecular dynamics simulation. The solvent contribution of the reorganization free energy is analyzed in terms of reorganization free energy densities and dipole reorientation densities. A ranking of amino acid residues according to reorganization free energy contribution is established and correlated to structural changes upon oxidation and self-exchange. Our results are concluded in section 4.

2. Computational Method

2.1. Diabatic Free Energies. The computation of diabatic free energy curves from molecular dynamics simulation has been reviewed in detail in our previous publications.[27−29] Here we define the reactions studied and give a summary of formulas that will be referred to in later sections. The system is composed of a four-helix bundle protein, two Ru−diphenylporphyrin cofactors (RuDPP) binding to the protein and solvent (aqueous ionic solution), and is denoted R = (II,II) in the reduced state and O = (III,II) in the oxidized state.

$$(\mathrm{II,II}) \rightarrow (\mathrm{III,II}) + 1\mathrm{e}^- \tag{2}$$

In the notation used in eq 2, the oxidation state of the first cofactor, POR1, is denoted by the first number and the oxidation state of the second cofactor, POR2, by the second number. Figure 1D gives a scheme of the amino acid sequence. For electron self-exchange,

$$(\mathrm{III,II}) \rightarrow (\mathrm{II,III}) \tag{3}$$

A = (III,II) is the reactant state and B = (II,III) the product state. The excess electron is located on POR2 in A and on POR1 in B.

The diabatic free energy curves for oxidation, eq 2, and self-exchange, eq 3, A_M, are obtained from the fluctuations or probability distribution, p_M, of the corresponding vertical energy gap ξ:

$$A_M(\xi') = -k_\mathrm{B}T \ln \Lambda^{-3N} \int \mathrm{d}\mathbf{R}^N \exp[-\beta E_M(\mathbf{R}^N)]\delta(\xi - \xi') \tag{4}$$

$$= -k_\mathrm{B}T \ln p_M(\xi') + \mathrm{const} \tag{5}$$

$$p_M(\xi') = \frac{\int \mathrm{d}\mathbf{R}^N \exp[-\beta E_M(\mathbf{R}^N)]\delta(\xi(\mathbf{R}^N) - \xi')}{\int \mathrm{d}\mathbf{R}^N \exp[-\beta E_M(\mathbf{R}^N)]} \tag{6}$$

In eqs 4−6, $\mathbf{R}^N$ denotes the configuration of all N atoms in the system, $\beta = 1/(k_\mathrm{B}T)$, T is the temperature, k_B is the Boltzmann constant, and Λ^{-3N} is the average thermal wavelength. In case of oxidation, $A_M = A_\mathrm{R},A_\mathrm{O}$ and $E_M = E_\mathrm{R},E_\mathrm{O}$. The vertical energy gap for oxidation is defined as

$$\xi(\mathbf{R}^N) := \Delta E_\mu(\mathbf{R}^N) = \Delta E_0(\mathbf{R}^N) + \mu \tag{7}$$

$$\Delta E_0(\mathbf{R}^N) = E_\mathrm{O}(\mathbf{R}^N) - E_\mathrm{R}(\mathbf{R}^N) \tag{8}$$

where E_O and E_R are the electronic ground-state energies of the oxidized protein O and the reduced protein R, and ΔE_0 is the vertical ionization energy (vertical electron affinity) if the nuclei move on the potential energy surface of R (O). The constant μ in eq 7 is the electronic chemical potential, which is set equal to minus the free energy difference between O and R,

$$\mu := -\Delta A \tag{9}$$

$$\Delta A = A_\mathrm{O} - A_\mathrm{R} = \frac{1}{2\beta}(-\ln\langle\exp(-\beta\Delta E_0)\rangle_\mathrm{R} + \ln\langle\exp(\beta\Delta E_0)\rangle_\mathrm{O}) \tag{10}$$

In eq 10, $\langle\cdots\rangle_M$ denotes the canonical average in state M. For this choice of μ, the driving force $\Delta A_\mu = \Delta A + \mu$ is equal to zero, which corresponds to zero overpotential in the experiment. In this case, the minima of the free energy curves, A_O and A_R, are exactly aligned, provided that the curvatures of the two profiles are equal. In the linear response approximation (LR), free energy difference and reorganization free energy are given by

$$\Delta A^\mathrm{LR} = {}^1/_2(\langle\Delta E_0\rangle_\mathrm{R} + \langle\Delta E_0\rangle_\mathrm{O}) \tag{11}$$

$$\lambda^\mathrm{LR} = {}^1/_2(\langle\Delta E_0\rangle_\mathrm{R} - \langle\Delta E_0\rangle_\mathrm{O}) \tag{12}$$

In the case of electron self-exchange, $A_M = A_\mathrm{A},A_\mathrm{B}$, $E_M = E_\mathrm{A},E_\mathrm{B}$, and

$$\xi(\mathbf{R}^N) := \Delta E(\mathbf{R}^N) = E_\mathrm{B}(\mathbf{R}^N) - E_\mathrm{A}(\mathbf{R}^N) \tag{13}$$

where $E_\mathrm{A} = E_\mathrm{O}$ and E_B is the potential energy after electron transfer. The free energy curves for electron self-exchange are symmetric, $A_\mathrm{B}(\Delta E) = -A_\mathrm{A}(\Delta E)$ and $\Delta A = 0$. In the linear response approximation, the reorganization free energy is given by the average energy gap:

$$\lambda^\mathrm{LR} = \langle\Delta E\rangle_\mathrm{A} \tag{14}$$

The free energy curves of the diabatic states are exactly related to one another by the linear free energy relation (see refs 28, 31, and 32),

$$A_\mathrm{O}(\Delta E_\mu) - A_\mathrm{R}(\Delta E_\mu) = \Delta E_\mu \tag{15}$$

$$A_\mathrm{B}(\Delta E) - A_\mathrm{A}(\Delta E) = \Delta E \tag{16}$$

Note that eqs 15 and 16 hold not only for Gaussian but for any distribution of the energy gap.

Gap energies are calculated using a classical force field model. Bonded and Lennard-Jones interactions remain unchanged upon oxidation and self-exchange. Therefore, only electrostatic interactions contribute to the gap energy:

$$\Delta E_0 = \sum_{i\in 1}\Delta q_i\left(\sum_{j\in N}\frac{q_j}{r_{ij}} + \sum_{j\in 2}\frac{q_j^\mathrm{R}}{r_{ij}} + \sum_{j\in 1\neq i}\frac{q_j^\mathrm{O} + q_j^\mathrm{R}}{2r_{ij}}\right) \tag{17}$$

$$\Delta E = \Delta E_2 - \Delta E_1 \tag{18}$$

where

$$\Delta E_I = \sum_{i\in I}\Delta q_i\left(\sum_{j\in N}\frac{q_j}{r_{ij}} + \sum_{j\in J}\frac{q_j^\mathrm{O}}{r_{ij}} + \sum_{j\in I\neq i}\frac{q_j^\mathrm{O} + q_j^\mathrm{R}}{2r_{ij}}\right) \tag{19}$$

$I = 2,1$, $J = 1,2$, $\Delta q_i = q_i^\mathrm{O} - q_i^\mathrm{R}$, and r_{ij} is the distance between atoms

(31) Warshel, A. *J. Phys. Chem.* **1982**, *86*, 2218.
(32) Tachiya, M. *J. Phys. Chem.* **1989**, *93*, 7050.

i and j. In eqs 17−19, we have divided the system into regions 1 and 2, composed of all ionizable atoms of cofactors 1 (POR1) and 2 (POR2) that have charge q_i^O in the oxidized state and charge q_i^R in the reduced state. Region N is comprised of the remaining atoms in the unit cell which have charge q_j in both states. The third term on the right-hand side of eqs 17 and 19 is the self-interaction contribution of the cofactor. The gap energy includes electrostatic interactions between atoms in the central unit cell only, whereas the electrostatic forces for MD are computed using Ewald summation. To account for the finite size of the simulation system, a correction term to the final reorganization free energy is applied using continuum theory (see section 3.5).

The diabatic free energy curves can be computed on the QM/MM level of theory by considering the difference between classical potential energy, E_M^{cl}, and QM/MM potential energy, $E_M^{QM/MM}$, as a bias potential ΔV:

$$p_M^{QM/MM}(\xi') = \langle \exp(\beta \Delta V(\xi)) \delta(\xi - \xi') \rangle_{E_M^{cl}} \quad (20)$$

$$\Delta V = E_M^{cl} - E_M^{QM/MM} \quad (21)$$

Equation 20 requires the computation of the QM/MM gap energies, eqs 7 respectively 13, for an ensemble of configurations sampled from classical molecular dynamics simulation. However, eq 20 gives the correct QM/MM gap distribution only if the configurational space sampled with classical and QM/MM simulations overlap sufficiently well. Although this is the case in the present simulations (see Table 2), we have not attempted to compute the gap distribution according to eq 20 (see discussion in section 3.5).

2.2. Simulation Details. Gas-Phase Calculations. Geometry optimizations of Ru−porphin (unsubstituted porphyrin, RuP) and Ru−porphin axially ligated with two pyridine molecules ($RuP(py)_2$) and two axial imidazole molecules ($RuP(im)_2$), respectively, were carried out using the Car−Parrinello code.[33] The reduced (Ru(II)) and oxidized states (Ru(III)) of RuP were optimized in D_{4h} symmetry for the triplet and quartet spin states, respectively. $RuP(py)_2$ and $RuP(im)_2$ were optimized in D_{2h} and C_{2h} symmetry, respectively, for the singlet spin state in the reduced form and for the doublet spin state in the oxidized form. The optimizations were carried out until the gradient of all atomic nuclei was smaller than 10^{-4} Hartree/bohr. This convergence criterion ensured that the displacement of nuclei in the last optimization step relative to the previous step was less than 10^{-4} bohr. The electronic orbitals were expanded in plane waves with a reciprocal kinetic energy cutoff of 70 Ry using BLYP[34,35] and BP[34,36] exchange-correlation functionals and norm-conserving pseudopotentials of the Troullier−Martins type.[37] Reference 29 gives specifications of the pseudopotential used for Ru, and ref 38 gives specifications of the pseudopotentials used for second-row elements. Vertical ionization potentials of the reduced states (IP) and vertical electron affinities of the oxidized states (EA) are calculated at the respective energy minimum structure.

QM/MM Simulation. The QM region is comprised of the porphyrin ring of cofactor POR1 and the two histidine residues HIS22 and HIS54, which ligate Ru in axial directions. All QM atoms are shown in Figure 1B. The two aryl substituents of POR1, the second RuDPP cofactor (POR2), the protein, and the aqueous solution are modeled with the AMBER 1999 force field[39] using the same system composition and atom topology as for classical simulations described below. The interaction between the QM system and the MM system is computed using a Hamiltonian electrostatic coupling scheme.[40] The electrostatic interaction energy between the electron + nuclei density of the QM subsystem and the point charges of all MM atoms within $r_{NN} = 15$ Å of any QM atom are calculated on a real space grid. All other MM atoms interact with RESP charges assigned to QM atoms. The latter are dynamically generated from the electron + nuclei density at each MD step.[41] The QM/MM boundary atoms, C_7^*,$C_7'^*$ of POR1 and the C_{12}^*, $C_{12}'^*$ (αC) atoms of HIS22 and HIS54 are described by monovalent pseudopotentials obtained by scaling the Troullier−Martins pseudopotential of carbon by a factor of 4. Test calculations performed with monovalent pseudopotentials and system parameters are summarized in the Supporting Information. QM/MM simulations were carried out with the CPMD code.[33] The initial configuration for the reduced state (II,II) was taken from a classical MD trajectory after equilibration for 1 ns at 300 K. During equilibration with classical MD, all atoms of POR1 and POR2 and all side-chain atoms of HIS22, HIS54, HIS86, and HIS118 were harmonically restrained to the position of a model structure[2] with a force constant 99 kcal/(mol Å) (see below). For equilibration with QM/MM, all position restraints were released. The bonds between terminating monovalent carbon atoms and QM atoms are fixed throughout equilibration and production runs at the equilibrium distances taken from the force field, $r(C_7^*-C_6) = r(C_7'^*-C_6') = 1.56$ Å and $r(C_{12}^*-C_{11}) = r(C_{12}'^*-C_{11}') = 1.54$ Å. During the first 0.5 ps of equilibration, the temperature of the system was rescaled to 300 K when it was outside the boundary 300 ± 5 K. A chain of Nose−Hoover thermostats[42] was then used with target temperature 300 K. After 5 ps of dynamics, the system temperature was 299.9 K, but the average temperature of the QM subsystem decreased to 269.0 K. Equilibration was continued for a further 1.2 ps using separate Nose−Hoover thermostats for QM atoms, protein, and water + ions. Retaining separate thermostating of the three subsystems, the next 5.5 ps of dynamics was taken to compute configurational averages. The QM/MM simulation of the oxidized state (III,II) was carried out similarly. Using the same initial structure as for the reduced complex and separate thermostats, the system was equilibrated at 300 K for 2.5 ps, and the next 5 ps of QM/MM dynamics was taken for statistical averages.

Classical MD Simulation. Classical MD simulations were carried out with the NAMD program[43] (Version 2.6b1) using the AMBER 1999 force field[39] for the protein and the TIP3P model for water.[44] The Ru−N interactions were modeled with bonding, electrostatic, and Lennard-Jones terms. Electrostatic interactions were computed using default atomic charges for all standard residues and restrained electrostatic potential (RESP)-derived charges for the RuDPP cofactor. The latter were obtained from DFT gas-phase calculations for the reduced and oxidized cofactor ligated with two methylimidazole ligands (see Figure 2). The RESP charges are given in the Supporting Information, together with details on force field and system parameters. The initial configuration of all non-hydrogen atoms of the protein and porphyrin cofactors was taken from a model structure.[2] The free valences were saturated with hydrogen atoms, and the protein was solvated with 5148 water molecules. All GLU side chains and terminal TYR residues were deprotonated, and all LYS side chains and terminal LEU residues were protonated according to protonation states at pH = 7. The system was neutralized by adding 14 Cl^- and 22 Na^+ ions, which amounts to a molality of 0.15 mol/kg in NaCl, a salt concentration typically used in experiments. The molality in four-helix bundle protein is 0.01 mol/kg, 3 orders of magnitude higher than under typical experimental conditions.

(33) *CPMD*, Version 3.10; The CPMD Consortium, MPI für Festkörperforschung, and the IBM Zurich Research Laboratory, 2005 (http://www.cpmd.org).
(34) Becke, A. D. *Phys. Rev. A* **1988**, *38*, 3098.
(35) Lee, C.; Yang, W.; Parr, R. *Phys. Rev. B* **1988**, *37*, 785.
(36) Perdew, J. P. *Phys. Rev. B* **1986**, *33*, 8822.
(37) Troullier, N.; Martins, J. *Phys. Rev. B* **1991**, *43*, 1993.
(38) Blumberger, J.; Klein, M. L. *Chem. Phys. Lett.* **2006**, *422*, 210.
(39) Case, D. A.; et al. *AMBER 7*; University of California, San Francisco, 2002.
(40) Laio, A.; VandeVondele, J.; Röthlisberger, U. *J. Chem. Phys.* **2002**, *116*, 6941.
(41) Laio, A.; VandeVondele, J.; Röthlisberger, U. *J. Phys. Chem. B* **2002**, *106*, 7300.
(42) Martyna, G. J.; Klein, M. L.; Tuckerman, M. *J. Chem. Phys.* **1992**, *97*, 2635.
(43) Phillips, J. C.; Braun, R.; Wang, W.; Gumbart, J.; Tajkhorshid, E.; Villa, E.; Chipot, C.; Skeel, R. D.; Kale, L.; Schulten, K. *J. Comput. Chem.* **2005**, *1781*, 26.
(44) Jorgensen, W. L.; Chandrasekhar, J.; Madura, J. D.; Impey, R. W.; Klein, M. L. *J. Chem. Phys.* **1983**, *79*, 926.

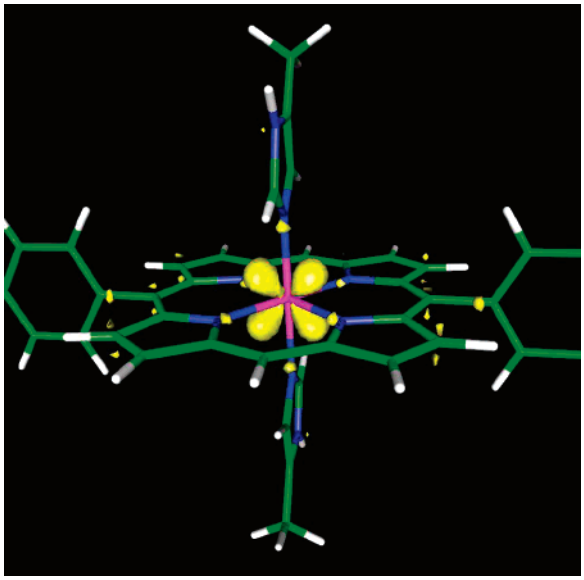

Figure 2. Electron density difference for oxidation of gas-phase Ru(II)DPP ligated with two methylimidazole molecules. The electron density difference is the difference between the ground-state electron densities of oxidized (Ru(III)) and reduced cofactor (Ru(II)) in the respective low-spin states at fixed ionic configuration. The calculations were carried out for the minimum energy configuration of the reduced state at the BP density functional level of theory using the CPMD code.[33] An isosurface of the electron density difference is depicted in yellow. The cofactor and ligands are shown in stick representation. Color code: H, white; C, green; N, blue; Ru, purple. The terminal carboxylate groups of the two aryl substituents were protonated. In the figure, only the phenyl rings of the aryl substituents are displayed; see Figure 1B for the full structure of RuDPP.

The atomic positions of the protein and cofactors were fixed at first, and the reduced solvated complex (II,II) was equilibrated for 1.3 ns using a MD time step of 1 fs, a barostat with target pressure 1.01325 bar, and a thermostat with target temperature 300 K. The atomic positions of the protein and cofactors were then restrained to the positions of the model structure with a force constant of 99 kcal/(mol Å), and the system was equilibrated for 1.2 ns using variable time steps between 0.2 and 2 fs and temperature rescaling to 300 K every 1000 MD steps. In the last 1 ns, the force constant for the restraint on protein atoms was reduced to 10 kcal/mol. Finally, all position restraints on the protein and cofactors were released, and the protein was equilibrated for a further 2.5 ns in the NPT ensemble using a time step of 2 fs. The next 10 ns of dynamics was taken for calculation of configurational averages. The classical MD simulation of the oxidized complex (III,II) was carried out similarly, using as initial geometry the last snapshot of the simulation of the reduced state where atomic positions were restrained to the model structure. After equilibration for 7 ns in the NPT ensemble, the next 10 ns of dynamics was taken for calculation of configurational averages.

3. Results and Discussion

3.1. Structure and Binding of Cofactor. Gas Phase. The results for gas-phase calculations at 0 K on model porphyrin systems are summarized in Table 1. The equatorial bond lengths $Ru-N_{eq}$ in Ru(II)P and Ru(II)P(py)$_2$ and the axial distances $Ru-N_{ax}$ in Ru(II)(py)$_2$ are well reproduced with the BP functional. The deviations relative to local basis set BP calculation[45] and crystal structure[46] are $\leq$0.01 Å, showing that the pseudopotentials used are sufficiently accurate. The equatorial distances are, on average, 0.01 Å longer when computed with the BLYP functional. More seriously, the axial bonds in Ru(II)P(py)$_2$ are overestimated by 0.05 Å relative to crystal structure. For this reason, we have chosen the BP functional for QM/MM calculations and parametrization of charges for the RuDPP cofactor. The change of bond lengths in response to oxidation of the metal is rather small. In RuP the equatorial bonds shrink by about 0.02 Å, while in Ru(II)P(im)$_2$ the equatorial and axial bond lengths change by less than 0.01 Å according to BP and BLYP density functional calculations. Modest changes in bond lengths, 0.01−0.02 Å, have also been reported for oxidation of Fe(II)P(im)$_2$[18] at the B3LYP level of theory.

Protein. Structural properties for the RuDPP cofactor binding to the four-helix bundle were obtained from QM/MM simulations at 300 K and are summarized in Table 2. Equatorial and axial Ru−N bonds augment on average by 0.01 and 0.02 Å, respectively, compared to the gas-phase model cofactor RuP(im)$_2$. The small increase of bond lengths is probably related to the finite temperature, indicating that the protein environment has little to no effect on the binding distances of the axial ligands. Similar to our result in the gas phase, the change of Ru−N bond lengths in response to oxidation is less than 0.01 Å. Modeling the Ru−N interactions with harmonic bonds, the classical MD simulations reproduce mean distances and root-mean-square fluctuations of QM/MM simulations to very good accuracy. The axial distances averaged over 10 ns are 0.01 Å larger and the equatorial distances 0.03 Å smaller than the values obtained from 5 ps of QM/MM dynamics (see Table 2). The use of bonding terms in the description of RuDPP−ligand interactions is essential in our model because simulations with purely electrostatic Ru−N interactions did not give a stable coordination (see Supporting Information for details).

3.2. Inner-Sphere Reorganization. A consequence of small changes in ligand binding distances is small inner-sphere reorganization energies. Contraction of the Ru−N bonds in RuP by 0.02 Å leads to a small gas-phase reorganization energy for self-exchange of $\lambda^i = 84$ meV at 0 K ($\lambda^i = IP - EA$), similar to that for RuP(im)$_2$, $\lambda^i = 88$ meV. Reorganization energies of the same magnitude are reported for FeP(im)$_2$, 85 meV,[18] and for ZnP, 50−98 meV,[19] both obtained at the B3LYP level of theory. Using photoelectron spectroscopy, Gray and co-workers[19] estimated the reorganization energy of gas-phase ZnP to be in the range 120−140 meV, suggesting that density functional calculations have the tendency to underestimate inner-sphere reorganization energies. However, a part of the discrepancy with experiment could also be due to finite temperature effects which are not included in the theoretical estimates.

Computation of inner-sphere reorganization free energies with QM/MM is fairly straightforward if only the first-shell ligands ("inner-sphere") are treated quantum mechanically. The QM/MM approach has the advantage that it accounts for finite temperature effects beyond the harmonic approximation and also for polarization of the inner-sphere electron cloud by the environment ("outer-sphere"). The inner-sphere reorganization energy of RuDPP bonded to the protein is expected to be small, similar to that of gas-phase RuP(im)$_2$, about 0.1 eV, because in the protein too, the Ru−N bond lengths are almost identical in the two oxidation states. Since inner-sphere reorganization energy is one order of magnitude smaller than outer-sphere reorganization energy, we have not further attempted to refine our gas-phase estimate of λ^i with QM/MM calculations.

(45) Liao, M.-S.; Scheiner, S. *Chem. Phys.* **2002**, *285*, 195.
(46) Hopf, F. R.; O'Brian, T. P.; Scheidt, W. R.; Whitten, D. G. *J. Am. Chem. Soc.* **1975**, *97*, 277.

Table 1. Summary of Gas-Phase Density Functional Calculations for Model Cofactors Ru−Porphin, Ru−Porphin Ligated with Two Pyridine Molecules, and Ru−Porphin Ligated with Two Imidazole Ligands, Carried out with the CPMD Code[33] for Reduced (M(II)) and Oxidized (M(III)) States (M = Ru)[a]

	RuP			$RuP(py)_2$			$RuP(im)_2$[f]		$FeP(im)_2$
	BP	BLYP	lit.	BP	BLYP	lit.	BP	BLYP	lit.[j]
				M(II)					
$Ru-N_{eq}$ (Å)	2.052	2.059	2.04[b]	2.063	2.071	2.06[b] 2.047[d,e]	2.054[g]	2.069	2.02
$Ru-N_{ax}$ (Å)				2.098	2.147	2.10[b] 2.100[d]	2.088	2.126	2.05
IP (eV)	6.283	6.067	6.27[b]	5.516	5.470	5.84[b]	5.375	5.092	
				M(III)					
$Ru-N_{eq}$ (Å)	2.026	2.046					2.053[h]	2.067[i]	2.01
$Ru-N_{ax}$ (Å)							2.090	2.130	2.03
EA (eV)	6.199	6.012					5.287	5.026	
λ^i (meV)	84	55	50−98[c]				88	66	85

[a] $Ru-N_{eq}$ is the bond length between Ru and the nitrogen atoms of the porphin ring, and $Ru-N_{ax}$ is the bond length between Ru and the nitrogen atom of the axial ligands. The vertical ionization potential is denoted IP, the vertical electron affinity EA, and the inner-sphere reorganization energy for self-exchange λ^i; λ^i = IP − EA. BP denotes Becke−Perdew, BLYP denotes Becke−Lee−Yang−Parr exchange correlation functional, and "lit." denotes literature values. See section 2.2 for further details. [b] BP, ref 45. [c] ZnP, B3LYP, ref 19. [d] Ru(II) octaethylporphyrindipyridinate crystal, ref 46. [e] Average of two bond lengths, 2.046 and 2.048 Å. [f] Optimized for a subgroup of C_{2h}. [g] Average of two bond lengths, 2.055 and 2.053 Å. [h] Average of two bond lengths, 2.061 and 2.045 Å. [i] Average of two bond lengths, 2.056 and 2.077 Å. [j] B3LYP, ref 18.

Table 2. Selected Bond Lengths, Angles, and Dihedral Angles of the RuDPP Cofactor Binding to the Four-Helix Bundle Protein at 300 K[a]

	QM	QM/MM	CMD	crystal[b]
		Ru(II)DPP		
$Ru-N_{ax}$	2.09	2.11 ± 0.06	2.12 ± 0.07	2.100
$Ru-N_{eq}$	2.05	2.06 ± 0.05	2.03 ± 0.06	2.047
$N_{eq}-C1$	1.38	1.39 ± 0.03	1.39 ± 0.03	1.367
C_1-C_2	1.45	1.45 ± 0.03	1.45 ± 0.03	1.45
C_2-C_3	1.37	1.37 ± 0.03	1.37 ± 0.02	1.32
C_1-C_5	1.40	1.40 ± 0.03	1.40 ± 0.03	1.40
C_2-H_1	1.09	1.09 ± 0.03	1.09	
C_3-H_2	1.09	1.09 ± 0.03	1.09	
C_5-H_3	1.09	1.10 ± 0.03	1.09	
$O-H_6$		2.12 ± 0.21	2.56 ± 0.37	
$\angle Ru-N_{ax}-C_8$	126.0	126.8 ± 3.8	128.2 ± 5.5	
$\angle C_9-N_{ax}-Ru-C_6$	2.7	34.5 ± 8.4	84.4 ± 8.8	
$\angle C_9'-N_{ax}'-Ru-C_6'$	−2.7	26.2 ± 7.7	33.6 ± 10.7	
$\angle C_9-N_{ax}-N_{ax}'-C_9'$	180	117.1 ± 11.8	62.2 ± 14.0	
		Ru(III)DPP		
$Ru-N_{ax}$	2.09	2.11 ± 0.06	2.12 ± 0.07	
$Ru-N_{eq}$	2.05	2.06 ± 0.05	2.03 ± 0.06	
$N_{eq}-C1$	1.38	1.39 ± 0.03	1.39 ± 0.03	
C_1-C_2	1.44	1.45 ± 0.03	1.45 ± 0.03	
C_2-C_3	1.37	1.37 ± 0.03	1.37 ± 0.02	
C_1-C_5	1.40	1.40 ± 0.03	1.40 ± 0.03	
C_2-H_1	1.09	1.09 ± 0.03	1.09	
C_3-H_2	1.09	1.09 ± 0.03	1.09	
C_5-H_3	1.09	1.10 ± 0.03	1.09	
$O-H_6$		2.04 ± 0.16	2.48 ± 0.36	
$\angle Ru-N_{ax}-C_8$	125.6	127.2 ± 4.1	128.7 ± 6.0	
$\angle C_9-N_{ax}-Ru-C_6$	3.3	34.7 ± 7.6	85.6 ± 9.0	
$\angle C_9'-N_{ax}'-Ru-C_6'$	−3.3	26.9 ± 8.2	23.9 ± 12.9	
$\angle C_9-N_{ax}-N_{ax}'-C_9'$	180	115.6 ± 9.9	70.3 ± 13.3	

[a] Mean values and root-mean-square fluctuations for Ru(II)DPP were obtained from QM/MM and classical molecular dynamics (CMD) simulation of the reduced form (II,II) and averaged over both cofactors. The values for Ru(III)DPP were obtained from QM/MM and CMD simulation of the oxidized form (III,II). QM/MM and CMD averages were calculated from trajectories of length 5 ps and 10 ns, respectively. Bond lengths obtained from gas-phase calculations at 0 K are summarized in column QM. $O-H_6$ denotes the bond between H_6 and the hydroxyl oxygen atom of the threonine residue in the vicinity of the cofactor. See Figure 1B for definition of all other atoms and section 2.2 for simulation details. Bond lengths are given in angstroms and angles in degrees. [b] Ru(II) octaethylporphyrindipyridinate crystal, ref 46.

Interestingly, the reorganization energy of $RuP(im)_2$ is one order of magnitude smaller than for the gas-phase hexaquo complex $Ru(H_2O)_6$, 0.82 eV.[28] While the large value for $Ru(H_2O)_6$ is due to contraction of Ru−O bond lengths by ∼0.08 Å, the small reorganization energy for $RuP(im)_2$ is achieved by covalent ring strain preventing the nitrogen atoms in the porphyrin plane from forming significantly shorter bonds with Ru in the oxidized state. This argument holds for the equatorial nitrogen atoms, but it is not valid for the axial ligands, which are free to respond to oxidation but contract by less than 0.01 Å. A first explanation of this observation is given by the fact that nitrogen forms rather soft and long bonds compared to oxygen or charged atoms, making them less susceptible to a change of charge of the central metal ion.[18]

3.3. Protein Dynamics. Histidine Ligands. On the time scale of present QM/MM simulations (5 ps), both axial histidine ligands are tightly bonded to Ru, with bond lengths fluctuating in the range 1.92−2.35 Å. The root-mean-square fluctuations of $Ru-N_{ax}$, 0.06 Å, and $Ru-N_{eq}$, 0.05 Å, are one order of magnitude larger than the change of Ru−N bond lengths upon oxidation. If solvent and protein motion were decoupled from ET, the self-exchange would be a spontaneous process and limited only by electronic coupling, which illustrates the high efficiency of porphyrin-based electron carriers.

Analyzing the QM/MM trajectory, we find that the histidine rings are not coplanar, as assumed in gas-phase optimizations, but rotated with respect to the $Ru-C_6$ and $Ru-C_6'$ axes by $\tau_1 = \angle C_9N_{ax}RuC_6 = 35°$ and $\tau_1' = \angle C_9'N_{ax}'RuC_6' = 26°$, respectively, giving an average dihedral angle $\tau_2 = \angle C_9N_{ax}N_{ax}'C_9' = 117°$ (see Table 2). Despite formation of a hydrogen bond between N_1-H_6 and the O−H group of a neighboring threonine residue, the histidine rings display large-amplitude oscillatory motion around the mean values, as can be seen from the root-mean-square fluctuations of about 10°. On the time scale of the present classical MD simulations, these fluctuations lead to frequent break and formation of the hydrogen bonds between histidine and threonine side chains, as indicated by the mean distance of about 2.5 Å (OH_6 in Table 2). Within 1 ns of classical MD, the floppy motion of one histidine ring culminates in a distinct rotation, leading to an increase of the dihedral τ_1 from 35° to 84° and a decrease of τ_2 from 117° to 62° until the end of the simulation (in total, 12.5 ns). The rotation of one

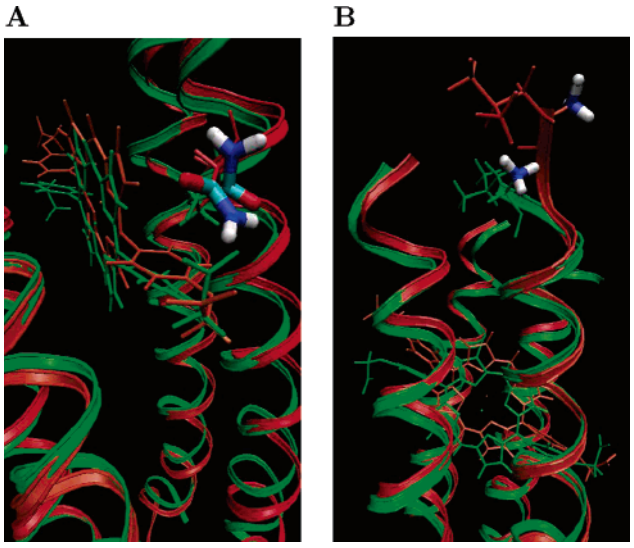

Figure 3. Response of GLN23 (A) and LEU97 (B) to oxidation of cofactor POR1. A snapshot taken from a classical MD trajectory in the oxidized state (orange) is projected on a snapshot taken from a trajectory in the reduced state (green). The four-helix bundle is depicted in ribbon representation, and POR1, GLN23, and LEU97 in stick representation. Relevant side-chain atoms of GLN23 and LEU97 are magnified and shown in atom-specific colors. Color code: H, white; C, green; N, blue; O, red. The carbonyl oxygen atom of the side chain of GLN23 points away from the porphyrin cofactor in the reduced state and points toward the cofactor in the oxidized state. The protonated terminal amino group of LEU97 becomes repelled upon oxidation.

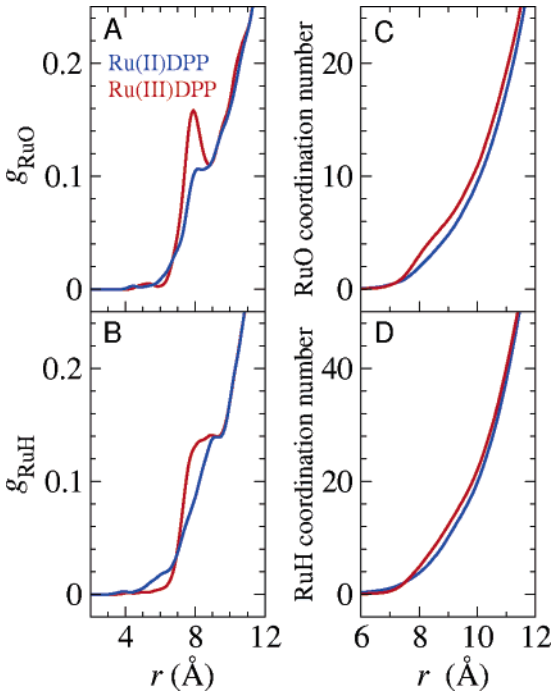

Figure 4. Radial distribution function $g(r)$ between Ru atom of cofactor POR1 and oxygen atoms (A), respectively hydrogen atoms (B), of the solvent. The distributions were obtained from 10 ns molecular dynamics simulation in state R ((II,II), blue lines) and O ((III,II), red lines) and were smoothed with a Gaussian. The oxygen and hydrogen coordination numbers of Ru obtained by spherical integration of the distributions are shown in panels C and D, respectively.

axial ligand is observed for both cofactors of the four-helix bundle and for both oxidation states.

Backbone. The helical structure around the porphyrin binding site is very stable, as indicated by the small root-mean-square deviation (rmsd) of the backbone atoms relative to the model structure,[2] 1.6 Å on average (see Figure 1 in the Supporting Information). This value is obtained for the backbone atoms of the helical core structure, excluding the last 8 residues at either end of the four helices. Inclusion of all but the last two N- and C-terminal residues of each helix leads to an increase of rmsd to 2.0 Å, while inclusion of all 32 residues/helix gives an rmsd of 2.3 Å. The increase in rmsd with chain length is due to increased flexibility of the last 8 or 10 residues, which allows for bending motion of the helices in this region. The fluctuations of the solvent-exposed terminal residues are particularly large, leading to partial unfolding and refolding of the terminal loops on the nanosecond time scale of the present simulations.

The change of rmsd in response to oxidation of the protein is small in the core region, $< +0.1$ Å, but larger when computed for all backbone atoms of the four-helix bundle, $+0.3$ Å relative to the reduced state. The slight increase in rmsd can be explained by the repulsion of the protonated N-terminal residues LEU97 and LEU33 upon increase of the total charge of the cofactor from 0 (Ru(II)) to 1 (Ru(III)) (see Figure 3B). The average length of the two antiparallel helices, measured between αC of LEU97 (LEU33) and carbonyl-C of TYR128 (TYR64), increases from 48.3 ± 1.9 (48.7 ± 1.5) to 50.3 ± 1.2 Å (49.8 ± 0.8 Å). Oxidation, therefore, leads to slight stretching of the two helices by 2.0 and 1.1 Å. This effect is smaller for the second antiparallel pair, <0.8 Å. The electrostatic repulsion of the two N-terminal residues is also manifested in the electron-transfer kinetics (see discussion in section 3.6). LEU33 and LEU97 are among the residues with the largest contribution to the reorganization free energy.

3.4. Protein Solvation. In Figure 4 we show the radial distribution functions between the Ru atom of the bound RuDPP cofactor and the oxygen, respectively hydrogen, atoms of the solvent. The onset of the distribution at about 6 Å comes from one or two water molecules that temporarily penetrate the four-helix bundle at the edges of the RuDPP cofactor. The hydrophobic interior of the protein is mostly free of solvent, except for certain times when water molecules penetrate the interhelical region between the two cofactors. The Ru−O radial distribution of the reduced cofactor integrates to 1 at 7.6 Å and to 4.5 at 8.9 Å and increases monotonically for distances larger than 9 Å.

Oxidation leads to a slight increase of the number of water molecules in the vicinity of the cofactor, as indicated by the appearance of a small peak at 7.9 Å which integrates to 5.8 at 8.9 Å. The solvent density is increased in the range 8−12 Å, followed by alternate and slight decrease and increase of density for higher solvation shells (note that the volume of the simulation system is virtually identical in the NPT ensembles of oxidized and reduced states). The increase of density between 8 and 12 Å is more than half as much for oxygen as for hydrogen (Figure 4C,D). This is probably related to dipole reorientation of the solvent upon oxidation, calculated to be −0.02 D/water molecule (see eq 26). The solvent reorganization has important consequences for energetics of oxidation and electron self-exchange and will be further discussed in section 3.6

3.5. Diabatic Free Energy Curves. Typical experimental reorganization free energies of natural porphyrin-based electron

Table 3. Convergence of the Root-Mean-Square Fluctuations of the Energy Gap for Self-Exchange, $\langle \delta \Delta E^2 \rangle^{1/2}$, and of the Reorganization Free Energy, λ^{LR}, as a Function of Simulation Time[a]

t (ns)	$\langle \delta \Delta E^2 \rangle^{1/2}$ (eV)	λ^{LR} (eV)
0.01	0.272	1.12
0.1	0.283	1.29
1	0.498	1.44
5	0.467	1.28
10	0.489	1.30

[a] The data were obtained from a classical molecular dynamics trajectory in state (III,II) by averaging over 1000 equidistant configurations within a simulation time t. ΔE and λ^{LR} were calculated according to eqs 18 and 14, respectively. The reasonably good agreement of λ^{LR} at 0.01 and 0.1 ns with the value at 10 ns is fortuitous due to a fortunate choice of initial conditions.

carriers are in the range 0.5−1.2 eV. The small inner-sphere contribution of about 0.1 eV (see section 3.2) implies that the total reorganization free energy is almost entirely provided by protein and solvent. For this reason, it is absolutely crucial to sample protein fluctuations sufficiently well. In Table 3 we show the root-mean-square fluctuation $\langle \delta \Delta E^2 \rangle^{1/2}$ of the electron-transfer energy, ΔE (eq 13), computed according to eq 18 for time scales ranging from 10 ps to 10 ns. On the typical time scale of the current QM/MM simulations, 10−100 ps, the fluctuations are just half the value obtained from 10 ns of classical dynamics. Sampling over several nanoseconds is clearly mandatory and probably sufficient, judging from the convergence of fluctuations and mean value (λ^{LR}, eq 14) on the nanosecond time scale. Considering the importance of sampling and the good performance of the classical force field (Table 2), we have used a purely classical electrostatic model to calculate the diabatic free energy curves for (i) oxidation of one of the two cofactors binding to the four-helix bundle (eq 2) and (ii) electron self-exchange (eq 3). The dependence of the results on the charge model will be discussed further below.

Oxidation. The gap energy for oxidation of (II,II) to (III,II) was calculated according to eqs 7 and 17 using the RESP charges parametrized for the two oxidation states. Converting the equilibrium fluctuations of the gap energy into free energies, eq 5, and extending the data points for each curve by virtue of eq 15, we find that the diabatic curves for oxidation are symmetric and very well approximated by parabolas, in agreement with Marcus theory (Figure 5A). From the quadratic fit functions we obtain a reorganization free energy $\lambda^{fit} = 0.78 \pm 0.03$ eV, in good agreement with the reorganization free energy obtained from the linear response formula (eq 12), $\lambda^{LR} = 0.74 \pm 0.02$ eV. The uncertainty of λ^{fit} is due to the choice of data points included in the fit (see Table 5), and the uncertainty of λ^{LR} represents the statistical error due to finite simulation length. Owing to eq 15, the full diabatic free energy curves can be constructed from just two equilibrium simulations without the need of enhanced sampling methods. This approach gives sufficient data points for the equilibrium region and for high excitations, yet sampling of the crossing region is not as good. The approximately linear behavior in the equilibrium and excited-state regions implies, however, that the quadratic fit functions provide a good interpolation of the free energy curves in the crossing region. This was indeed the case for aqueous Ag^+/Ag^{2+}, despite the moderate deviations from linear response that we have found for this redox pair.[27]

The reorganization free energy of 0.78 eV includes the contributions of the cofactors, protein, and ∼5000 explicit water

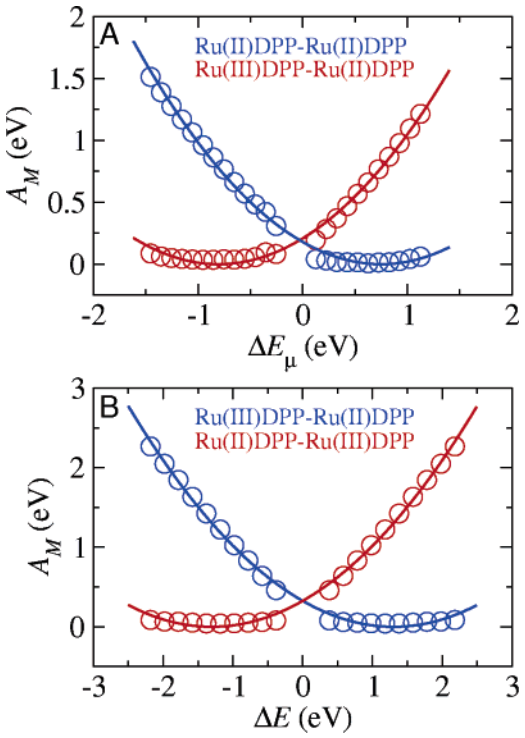

Figure 5. (A) Diabatic free energy curves for oxidation of the porphyrin cofactor POR1 binding to the four-helix bundle protein (eq 2). The electronic chemical potential μ was set equal to $-\Delta A$ (calculated according to eq 10), which corresponds to zero overpotential. The two sets of data points in the low-energy region of R (blue) and O (red) were obtained by collecting data points within 2 standard deviations of the mean value of the gap ΔE_μ in bins of width 0.1 eV and calculation of the free energy according to eq 5. The two sets of data points in the high-energy region of R and O were obtained by applying the linear free energy relation (eq 15). The set for R was obtained by shifting data points in the low-energy region of O by $-\Delta E_\mu$, and the set for O was obtained by shifting data points in the low-energy region of R by ΔE_μ. The combined set of data points was fitted to a parabola. (B) Diabatic free energy curves for electron self-exchange between two porphyrin cofactors, POR1 and POR2, binding to the four-helix bundle protein (eq 3). Data points within 2 standard deviations of the mean value of the gap ΔE were collected in bins of width 0.1 eV, and the corresponding free energy was evaluated according to eq 5 (circles in the low-energy region). Data points for high excitations are obtained similarly as in panel A, using the linear free energy relation (eq 16). The combined set of data points was fitted to a parabola. See also Table 5.

molecules but not the contribution from the bulk solvent. The latter can be estimated using a continuum approximation,[9,22] $\lambda^{bulk}/\text{eV} = (14.397/2)(1/\epsilon_\infty - 1/\epsilon_w)(1/r)$, where ϵ_∞ is the high-frequency dielectric constant of bulk water, ϵ_w the static dielectric constant of water, and r the radius of the solute in angstroms. Assuming $\epsilon_\infty = 2$, $\epsilon_w = 80$, and a radius r in the range 25−34.9 Å, we find an estimate for reorganization free energy of $\lambda^{bulk} = 0.10-0.14$ eV. As simulations were carried out for a cubic unit cell, an effective range for r was approximated as follows: the lower bound, $r = 25$ Å, was taken to be the distance between Ru and the nearest edge of the box (i.e., excluding the water molecules in the corners of the box); the upper bound, $r = 34.9$ Å, corresponds to the radius of a sphere that has the same volume as the cubic unit cell used in simulations. The lower bound overestimates the bulk contribution and therefore provides an upper bound for λ^{bulk} and vice versa. Due to the $1/r$ relation, λ^{bulk} depends only little on the choice of r in this range of (rather large) distances. The total reorganization free energy is then estimated to be $\lambda_{tot} = \lambda^{fit} + \lambda^{bulk} = 0.78 + 0.12 = 0.90 \pm 0.04$ eV. The uncertainty accounts

Table 4. Reorganization Free Energies for Oxidation of a Ru(II)DPP Cofactor Binding to the Four-Helix Bundle Protein (Eq 2)[a]

	RESP	RESPm2
λ^{fit} (eV)[b]	0.78 ± 0.03	0.78 ± 0.03
λ^{LR} (eV)[c]	0.74 ± 0.02	0.74 ± 0.02
λ_{tot} (eV)[d]	0.90 ± 0.04	0.90 ± 0.04
$\lambda_{\mathrm{tot}}^{\mathrm{LR}}$ (eV)[e]	0.86 ± 0.03	0.86 ± 0.03
λ^{i} (eV)[f]	−0.01	0.00
λ^{o} (eV)[g]	0.87	0.86
λ^{p} (eV)[h]	0.27	0.27
λ^{w} (eV)[i]	0.48	0.47
λ^{bulk} (eV)[j]	0.12 ± 0.02	0.12 ± 0.02
$\langle \Delta E_0 \rangle_{\mathrm{R}}$ (eV)[k]	1.66 ± 0.03	0.94 ± 0.03
$\langle \Delta E_0 \rangle_{\mathrm{O}}$ (eV)[k]	0.18 ± 0.02	−0.54 ± 0.02
$\langle \delta\Delta E_0^2 \rangle_{\mathrm{R}}^{1/2}$ (eV)	0.287	0.294
$\langle \delta\Delta E_0^2 \rangle_{\mathrm{O}}^{1/2}$ (eV)	0.301	0.306
ΔE_{R} (eV)	0.75	0.76
ΔE_{O} (eV)	−0.81	−0.80
ΔA (eV)[l]	1.02 ± 0.02	0.26 ± 0.02
ΔA^{LR} (eV)[m]	0.92 ± 0.02	0.20 ± 0.02
ΔA_{μ} (eV)	0	0
$\Delta A_{\mu}^{\ddagger}$ (eV)[n]	0.23 ± 0.01	0.23 ± 0.01

[a] The free energies were obtained from the fluctuations of the electrostatic energy gap ΔE_0, which is defined in eq 8 and computed according to eq 17 using (i) RESP charges for R and O ("RESP") and (ii) RESP charges for R and RESPm2 charges for O cofactor ("RESPm2"); see Table 1 in the Supporting Information. $\langle \Delta E_0 \rangle_M$ and $\langle \delta\Delta E_0^2 \rangle_M^{1/2}$ denote mean value and root-mean-square fluctuations of ΔE_0 averaged over 10 ns of molecular dynamics in state M = R,O. The minima of the parabolic fits of the diabatic free energy curves (Figure 5A) are denoted ΔE_M. [b] Obtained from parabolic fit of data shown in Figure 5A; uncertainty of fit taken from Table 5. [c] Linear response estimate, eq 12. [d] Bulk corrected, $\lambda_{\mathrm{tot}} = \lambda^{\mathrm{fit}} + \lambda^{\mathrm{bulk}}$. [e] Bulk corrected, $\lambda_{\mathrm{tot}}^{\mathrm{LR}} = \lambda^{\mathrm{LR}} + \lambda^{\mathrm{bulk}} = \lambda^{\mathrm{i}} + \lambda^{\mathrm{o}}$. [f] Inner-sphere reorganization free energy estimated from a classical point charge model using LR approximation. It is comprised of contributions from POR1, HIS22, and HIS54, see Table 7. [g] Outer-sphere reorganization free energy estimated from classical point charge model using LR approximation, $\lambda^{\mathrm{o}} = \lambda^{\mathrm{p}} + \lambda^{\mathrm{w}} + \lambda^{\mathrm{bulk}}$. [h] Sum of reorganization free energy contributions of all protein residues excluding HIS22 and HIS54, see Table 7. [i] Sum of reorganization free energy contributions of all water molecules ("wat") and solvated ions ("ions"), see Table 7. [j] Estimated as explained in section 3.5. [k] Statistical error = $(s/N)^{1/2} \langle \delta\Delta E_0^2 \rangle_M^{1/2}$, where s is the statistical inefficiency and N the number of data points.[58] [l] Equation 10. [m] Equation 11. [n] $\Delta A_{\mu}^{\ddagger} = \lambda_{\mathrm{tot}}/4$.

for the error due to data fit, simulation length, bulk contribution, and charge model: $\pm(0.03^2 + 0.02^2 + 0.02^2 + 0.004^2)^{1/2} = \pm 0.04$ eV.

An important question that has to be addressed concerns the sensitivity of our results to the particular choice of charges used to compute the gap energies. According to the RESP charge model used, all atoms of the porphyrin and of the histidine side chains contribute to the oxidation process, i.e., have a more positive charge in the oxidized state (see Table 1 in the Supporting Information). Note that this is a consequence of the RESP charge model not reflecting the actual ionization process, which occurs primarily at the site of Ru according to experiment and BP density functional calculations (see electron density difference in Figure 2). To investigate the sensitivity of free energies to excess charge distribution, we have computed the diabatic curves for a model where ionization takes place entirely on the Ru ion. The charge of Ru is increased by 1 upon oxidation, while the charges of all the other atoms of the cofactor and ligands remain unchanged (charge set "RESPm2"). This is at the other extreme of delocalized excess charge distribution, as implied by the RESP charge model. As one can see in Table 4, the fluctuations of the energy gap remain almost unchanged if the RESPm2 charges are used. The change in reorganization free energy is less than 0.01 eV relative to the RESP charge model. The insensitivity of reorganization energy to distribution of excess charge is due to the large average separation distance between the parts of the system that contribute most to reorganization (solvent and protein) and the center of ionization, typically 10−25 Å. The reorganizing part of the system "feels" only the total change in charge, and the detailed distribution of excess charge is less important. This is also the reason why we do not expect any major changes in reorganization free energy when computed at the level of QM/MM according to eq 20.

Interestingly, our estimate for reorganization free energy of oxidation, 0.78 eV (without bulk contribution), is almost identical with the value obtained by Simonson for oxidation of yeast cyt c, 0.77 eV.[26] Experimental values determined from electrochemical measurements for cytochromes are somewhat lower and range from 0.43 ± 0.02 eV for cyt b5[47] to 0.58 ± 0.03,[47] 0.6 ± 0.02,[48] and 0.62 ± 0.04 eV[30] for cyt c, even though a range of larger values was estimated in ref 49, 0.6−0.8 eV. Reorganization free energies for oxidation of porphyrin-binding four-helix bundles have not been measured but are roughly estimated to be about 1 eV.[1,50] This estimate is in good agreement with our calculated value that includes bulk solvation, 0.90 ± 0.04 eV. However, since solvation of the protein in the vicinity of the electrode is less effective than that in bulk solution, one would expect that the experimental value is lower than our calculated estimate. Assuming only small effects from electric field[51] and redox mediators,[49] the measured reorganization free energy for oxidation of the four-helix bundle might be smaller than estimated in ref 1 and closer to the values measured for native cytochromes, possibly in the range 0.6−0.8 eV.

Self-Exchange. The diabatic free energy curves for electron self-exchange, obtained from the fluctuations of the energy gap ΔE (eq 13), are shown in Figure 5B. Since reactant and product are identical, the curves are symmetric and the minima are aligned, $\Delta A = 0$ eV. The profiles are well approximated by parabolas, and the reorganization free energy obtained from the parabolic fit, $\lambda^{\mathrm{fit}} = 1.30$ eV, is virtually identical with the linear response estimate, λ^{LR}, of eq 14. The reorganization free energy is again rather insensitive to the modeling of the excess charge (0.06 eV difference relative to RESPm2 charge model; see Table 6). Bulk contributions are expected to be smaller for self-exchange than for oxidation, because in the former the bulk solvent responds to a change of dipole moment while in the latter it responds to a change of total charge. Assuming a bulk contribution half as large as the one for oxidation, $\lambda^{\mathrm{bulk}} = 0.06 \pm 0.03$ eV, and uncertainties of ±0.01 eV for data fit (Table 5), ±0.05 eV for finite simulation time, and ±0.06 eV for modeling of excess charge, we obtain a final value of $\lambda_{\mathrm{tot}} = \lambda^{\mathrm{fit}} + \lambda^{\mathrm{bulk}} = 1.36 \pm 0.08$ eV. The reorganization free energy for self-exchange is 1.5 times larger than for oxidation due to a change of charge in two cofactors.

(47) Blankman, J. I.; Shahzad, N.; Dangi, B.; Miller, C. J.; Guiles, R. D. *Biochemistry* **2000**, *39*, 14799.
(48) Fedurco, M.; Augustynski, J.; Indiani, C.; Smulevich, G.; Antalík, M.; Bánó, M.; Sedlák, E.; Glascock, M. C.; Dawson, J. H. *J. Am. Chem. Soc.* **2005**, *127*, 7638.
(49) Khoshtariya, D. E.; Dolidze, T. D.; Sarauli, D.; van Eldik, R. *Angew. Chem., Int. Ed.* **2006**, *45*, 277.
(50) Topoglidis, E.; Discher, B. M.; Moser, C. C.; Dutton, P. L.; Durrant, J. *ChemBioChem* **2003**, *4*, 1332.
(51) Rose, D. A.; Benjamin, I. *Chem. Phys. Lett.* **1995**, *234*, 209.

Table 5. Dependence of Reorganization Free Energy, λ^{fit}, on Data Points Used for the Parabolic Fits Shown in Figure 5A for Oxidation and in Figure 5B for Electron Self-Exchange[a]

		λ^{fit} (eV)	
σ	$A_m(1/k_BT)$	self-exchange	oxidation
1.0	<1	1.31	0.78
1.5	1	1.29	0.75
2.0	2	1.30	0.78
2.5	3	1.29	0.77

[a] Data points within $\pm\sigma$ of the mean value of the energy gap equilibrium distributions are used for the parabolic fit. The corresponding maximum free energy excitation is denoted A_m and given in units of thermal energy at $T = 300$ K.

Reorganization free energies for self-exchange in the four-helix bundle have not been measured, but experimental data are available for interprotein ET in cytochrome complexes: $\lambda = 0.5$ eV for cyt c551/cyt c55,[52] 0.69−0.8 eV for cyt c/cyt c,[11,53,54] 1.06−1.2 eV for cyt b5/cyt b5,[53,54] and 1.2−1.3 eV for cyt b5/cyt b5 mutants.[55] The theoretical estimate of 1.36 ± 0.08 eV for the four-helix bundle is slightly larger than the upper end of the range of experimental estimates and closest to the experimental value for cyt b5. We note that the reorganization free energy calculated here for a nonpolarizable point charge model might decrease to somewhat smaller values if electronic polarization is explicitly included in the calculation.[25,56] This can be inferred from the $(1/\epsilon_\infty - 1/\epsilon_0)$ dependence of the reorganization free energy on the high-frequency dielectric constant ϵ_∞, $\epsilon_\infty \approx 1.5-2$ for water. The nonpolarizable TIP3P model and AMBER 1999 force field ($\epsilon_\infty = 1$) account for electronic polarization but only implicitly through scaled effective charges. Unfortunately, there is no polarizable force field available that can be readily applied to the system studied. A common method for treating electronic polarization explicitly is to rescale the force field charges and assign empirical polarizabilities to each atom type.[25] Linear scaling DFT-based electronic structure methods that can handle several thousand atoms quantum mechanically are certainly a more reliable tool to investigate electronic polarization effects.[57] These rather demanding calculations are out of the scope of the present paper but will be the focus of future work.

3.6. Outer-Sphere Reorganization. The total reorganization free energy was estimated in section 3.5 to be 0.90 eV for oxidation and 1.36 eV for self-exchange. This is more than one order of magnitude larger than the estimate for inner-sphere reorganization (see section 3.2). Naturally, the question arises about the origin of the large outer-sphere contribution. Using the linear response approximation, we have calculated the contributions λ_r of protein residues and explicitly treated water molecules to determine the reorganization free energy for oxidation, $\lambda_r = (\langle \Delta E_{0,r}\rangle_R - \langle \Delta E_{0,r}\rangle_O)/2$, and electron self-exchange, $\lambda_r = (\langle \Delta E_r\rangle_A - \langle \Delta E_r\rangle_B)/2$, where $\Delta E_0 = \sum_r \Delta E_{0,r}$, $\Delta E = \sum_r \Delta E_r$, and $\lambda^{LR} = \sum_r \lambda_r$. The contributions λ_r are further divided into charge−charge and charge−dipole reorganization free energies, λ_{qq} and $\lambda_{q\mu}$,

$$\lambda_{qq} = q_r(\langle 1/d_1\rangle_R - \langle 1/d_1\rangle_O)/2 \quad (22)$$

$$\lambda_{q\mu} = (\langle \vec{\mu}_r\cdot\vec{d}_1/d_1^3\rangle_R - \langle \vec{\mu}_r\cdot\vec{d}_1/d_1^3\rangle_O)/2 \quad (23)$$

for oxidation and

$$\lambda_{qq} = q_r(\langle \Delta V_r^c\rangle_A - \langle \Delta V_r^c\rangle_B)/2 \quad (24)$$

$$\lambda_{q\mu} = (\langle \Delta E_r^d\rangle_A - \langle \Delta E_r^d\rangle_B)/2 \quad (25)$$

for self-exchange, where $\Delta V_r^c = 1/d_2 - 1/d_1$, $\Delta E_r^d = \vec{\mu}_r\cdot\vec{d}_2/d_2^3 - \vec{\mu}_r\cdot\vec{d}_1/d_1^3$, q_r and $\vec{\mu}_r$ are the charge and dipole moments of residue r, $\vec{d}_i$ is the vector between the center of mass of residue r and the center of mass of all ionizable atoms of cofactor i, and $d_i = |\vec{d}_i|$, $i = 1,2$. For large separation distances, $\lambda_r \approx \lambda_{qq} + \lambda_{q\mu}$.

Oxidation. The analysis of outer-sphere contributions for oxidation is summarized in Table 4, and a ranking of residues according to their contributions is given in Table 7. We find that the aqueous ionic solution contributes most, $\lambda^w + \lambda^{bulk} = 0.48 + 0.12 = 0.60$ eV, or 69% to the total outer-sphere reorganization free energy λ^o, $\lambda^o = \lambda^p + \lambda^w + \lambda^{bulk} = 0.87$ eV.

Table 6. Reorganization Free Energy for Electron Self-Exchange between Two RuDPP Cofactors Binding to the Four-Helix Bundle (Eq 3)[a]

	RESP	RESPm2
λ^{fit} (eV)[b]	1.30 ± 0.01	1.36 ± 0.05
λ^{LR} (eV)[c]	1.30 ± 0.05	1.32 ± 0.05
λ_{tot} (eV)[d]	1.36 ± 0.08	1.42 ± 0.09
λ_{tot}^{LR} (eV)[e]	1.36 ± 0.08	1.38 ± 0.08
λ^i (eV)[f]	0.09	0.12
λ^o (eV)[g]	1.27	1.26
λ^p (eV)[h]	0.59	0.58
λ^w (eV)[i]	0.62	0.62
λ^{bulk} (eV)[j]	0.06 ± 0.03	0.06 ± 0.03
$\langle \Delta E\rangle_A$ (eV)[k]	1.30 ± 0.05	1.32 ± 0.05
$\langle \delta\Delta E^2\rangle_A^{1/2}$ (eV)	0.489	0.498
ΔE_A (eV)	1.30	1.36
ΔA (eV)	0	0
$\Delta A^{\ddagger}$ (eV)[l]	0.34 ± 0.02	0.36 ± 0.02

[a] The free energies were obtained from the fluctuations of the electrostatic energy gap, ΔE, which is defined in eq 13 and computed according to eq 18 using (i) RESP charges for reduced and oxidized cofactors ("RESP") and (ii) RESP charges for the reduced and RESPm2 charges for the oxidized cofactor ("RESPm2"); see Table 1 in the Supporting Information. $\langle \Delta E\rangle_A$ and $\langle \delta\Delta E^2\rangle_A^{1/2}$ denote mean value and root-mean-square fluctuations of ΔE averaged over 10 ns of molecular dynamics in state A. The minimum of the parabolic fit of the diabatic free energy curve (Figure 5B) is denoted ΔE_A. [b] Obtained from parabolic fit of data shown in Figure 5B; uncertainty of fit taken from Table 5. [c] Linear response estimate, eq 14. [d] Bulk corrected, $\lambda_{tot} = \lambda^{fit} + \lambda^{bulk}$. [e] Bulk corrected, $\lambda_{tot}^{LR} = \lambda^{LR} + \lambda^{bulk} = \lambda^i + \lambda^o$. [f] Inner-sphere reorganization free energy estimated from a classical point charge model using LR approximation. It is comprised of contributions from POR1, POR2, HIS22, HIS54, HIS86, and HIS118, see Table 8. [g] Outer-sphere reorganization free energy estimated from classical point charge model using LR approximation, $\lambda^o = \lambda^p + \lambda^w + \lambda^{bulk}$. [h] Sum of reorganization free energy contributions of all protein residues excluding HIS22, HIS54, HIS86, and HIS118, see Table 8. [i] Sum of reorganization free energy contributions of all water molecules ("wat") and solvated ions ("ions"), see Table 8. [j] Estimated as explained in section 3.5. [k] Statistical error $= (s/N)^{1/2}\langle \delta\Delta E^2\rangle_A^{1/2}$, where s is the statistical inefficiency and N the number of data points.[58] [l] $\Delta A^{\ddagger} = \lambda_{tot}/4$.

(52) Dixon, D. W.; Hong, X. *Adv. Chem. Ser.* **1990**, *226*, 161.
(53) Dixon, D. W.; Hong, X.; Woehler, S. E.; Mauk, A. G.; Sishta, B. P. *J. Am. Chem. Soc.* **1990**, *112*, 1082.
(54) Andrew, S. M.; Thomasson, K. A.; Northrup, S. H. *J. Am. Chem. Soc.* **1993**, *115*, 5516.
(55) Ma, D.; Wu, Y.; Qian, C.; Tang, W.; Wang, Y.-H.; Wang, W.-H.; Lu, J.-X.; Xie, Y.; Huang, Z.-X. *Inorg. Chem.* **1999**, *38*, 5749.
(56) Ceccarelli, M.; Marchi, M. *J. Phys. Chem. B* **2003**, *107*, 5630.
(57) *Quickstep*; CP2K Developers Group (http://cp2k.berlios.de).
(58) Allen, M. P., Tildesley, D. J., Eds. *Computer Simulation of Liquids*; Clarendon Press: Oxford, 2000.

Table 7. Ranking of Residues According to the Reorganization Free Energy Contribution λ_r for Oxidation of the RuDPP Cofactor (POR1)[a]

rank	residue	λ_r (meV)	λ_{qq} (meV)	$\lambda_{q\mu}$ (meV)	charge (e)	$\langle d_1\rangle_R$ (Å)	$\Delta\langle d_1\rangle$ (Å)	$\Delta\langle p^{\parallel}\rangle$ (D)
1	wat	564	0	552	0	29.8	0.12	−0.02
2	GLN112	39	0	14	0	10.3	−0.68	−1.15
3	GLN23	36	0	51	0	8.0	−0.29	−2.07
4	GLN55	29	0	35	0	7.5	0.07	−1.29
5	LEU97	27	56	−29	1	17.4	2.65	4.51
6	GLN73	24	0	23	0	8.7	0.09	−1.13
7	GLU67	23	12	15	−1	17.2	−0.50	−3.29
8	GLN80	22	0	20	0	10.0	0.99	−0.71
9	LYS21	21	14	18	1	11.1	0.25	−2.08
10	LYS95	17	7	10	1	31.3	0.98	−6.20
11	GLN102	15	0	19	0	13.6	−0.54	−2.03
12	ALA72	13	0	8	0	7.2	0.00	−0.28
13	LYS85	13	18	−5	1	18.4	0.88	1.26
14	HIS22	9	−7	22	0.268	4.8	−0.05	0.31
15	LYS117	9	6	4	1	18.4	0.27	−0.83
16	LYS127	9	11	−2	1	30.2	1.50	2.09
17	HIS54	8	−4	22	0.268	4.9	−0.03	0.33
122	POR2	−8	−18	−1	−2.537	16.9	0.29	0.29
131	POR1	−34			−2.537	0.3	0.05	0.12
132	ions	−83	−84	0	8	32.5	0.26	0.00

[a] λ_r is decomposed into charge−charge and charge−dipole contributions, λ_{qq} (eq 22) and $\lambda_{q\mu}$ (eq 23), respectively; $\lambda_r \approx \lambda_{qq} + \lambda_{q\mu}$ for large distances $\langle d_1\rangle_R$. Charge refers to the total charge of each residue. The average distance between the center of mass of a residue and the center of mass of all ionizable atoms of cofactor POR1 is denoted $\langle d_1\rangle_R$, and the change of average distance upon oxidation is $\Delta\langle d_1\rangle = \langle d_1\rangle_O - \langle d_1\rangle_R$. The dipole reorientation upon oxidation, $\Delta\langle p^{\parallel}\rangle$, was calculated according to eq 26. "wat" refers to the sum of contributions of all water molecules and "ions" to the sum of contributions of all sodium and chloride ions in the system. The distances for "wat" ("ions") are averaged over all water molecules (ions) in the system, and $\Delta\langle p^{\parallel}\rangle$ is the average per water molecule. Only the first 16 of 128 amino acid residues are listed.

$\lambda^w = \lambda_r^{wat} + \lambda_r^{ions}$ is the contribution of all explicitly simulated water molecules and ions given in Table 7. The protein reorganization free energy, $\lambda^p = 0.27$ eV (31%), is spread over many amino acids (see Table 7). The residue with the highest contribution is GLN112, $\lambda_r = 39$ meV, followed by GLN23, GLN55, and LEU97, with values of 36, 29, and 27 meV, respectively. The contribution of the axial histidine ligands to the inner-sphere energy λ^i is very small, <10 meV. The "ranking" of residues with respect to λ_r does not correlate with the distance between the residue and the oxidized cofactor (POR1), $\langle d_1\rangle_R$, nor with charge or dipole moment of the amino acids. However, all residues ranked in the top 10 have charged (LYS,GLU) or dipolar (GLN) side chains or are charged terminal residues (LEU). Highly ranked dipolar amino acids are located in the vicinity of POR1, $\langle d_1\rangle_R \leq 10$ Å, whereas highly ranked charged amino acids can be separated from POR1 by more than 30 Å (LYS95). The contribution of distant but charged residues is a consequence of poor screening of electrostatic interactions in the hydrophobic interior of the four-helix bundle.

Reorganization free energies originate from structural changes in response to vertical ionization or electron transfer. Highly ranked dipolar amino acids are expected to exhibit significant changes in orientation of their dipoles, while charged amino acids are expected to change the distance to the cofactor. This is indeed the case. As one can see in Figure 3A, the carbonyl oxygen atom of the side chain of GLN23 points away from POR1 in the reduced state. Upon oxidation, the side chain rotates and the carbonyl oxygen atom points toward the cofactor. We have made this observation more quantitative and calculated the dipole reorientation $\Delta\langle p^{\parallel}\rangle$ for each residue (see Table 7):

$$\Delta\langle p^{\parallel}\rangle = \langle p^{\parallel}\rangle_O - \langle p^{\parallel}\rangle_R \tag{26}$$

$$p^{\parallel} = \vec{\mu}_r \cdot \vec{d}_1/d_1 \tag{27}$$

With the exception of LEU97, $\Delta\langle p^{\parallel}\rangle$ is negative for all residues ranked in the top 10, showing that the dipoles reorganize upon oxidation in antiparallel direction relative to POR1. The magnitude of dipole reorientation is in the range 1−6 D, to be compared with the permanent dipole moment of 2.35 D in the TIP3P model for water. The reorganization of the protonated N-terminal residue LEU97 is remarkably different. The distance between LEU97 and POR1 increases upon oxidation by $\Delta\langle d_1\rangle = \langle d_1\rangle_O - \langle d_1\rangle_R = 2.7$ Å, leading to a charge−charge reorganization free energy of 56 meV (see Figure 3B). By contrast, dipolar reorientation lowers the reorganization free energy by 29 meV, to 27 meV ($\Delta\langle p^{\parallel}\rangle = +4.5$ D).

According to the analysis presented, the solvent provides more than two-thirds of the reorganization free energy. Is this dominant contribution associated with the reorganization of a few water molecules in the vicinity of the cofactor or related to a more global response of the solvent? We have investigated this question by calculating the radial reorganization free energy density of water,

$$\rho_\lambda(d_1) = \mathrm{d}\,\lambda_{q\mu}(d_1)/\mathrm{d}\,d_1 \tag{28}$$

where $\lambda_{q\mu}(d_1)$ is the reorganization free energy of all water molecules within a distance d_1 measured between the center of mass of a water molecule and the center of mass of all ionizable atoms of cofactor POR1 (computed using the dipole approximation, eq 23). The density $\rho_\lambda(d_1)$ illustrated in Figure 6A represents the total reorganization free energy of all water molecules in a spherical shell of width 1 Å centered at a distance d_1. Note that integration of $\rho_\lambda(d_1)$ over the unit cell gives the total reorganization free energy of water (without bulk contribution), $\int_{cell} \mathrm{d}\,d_1\rho_\lambda(d_1) = \lambda_{q\mu}^{wat} = 0.552$ eV (see inset of Figure 6A). The radial dipole reorientation density corresponding to $\rho_\lambda(d_1)$,

$$\rho_p(d_1) = \langle \mathrm{d}\,p^{\parallel}(d_1)/\mathrm{d}\,d_1\rangle_O - \langle \mathrm{d}\,p^{\parallel}(d_1)/\mathrm{d}\,d_1\rangle_R \tag{29}$$

is illustrated in Figure 6B.

The distribution of ρ_λ is broad and exhibits several peaks in the range 6−40 Å, indicating that the response of the solvent extends far beyond the first solvation shells of the protein. The first peak is centered at 8 Å and integrates to 0.11 eV at 9 Å. This contribution is due to the increased number of water molecules from 4.5 to 5.8 in the vicinity of the cofactor (see Figure 4C ($r \approx d_1$) and section 3.4) as well as reorientation of water dipoles (Figure 6B). The second and highest peak is centered at 12 Å and corresponds to the first solvation shells with increased water molecule density (see Figure 4C and section 3.4). Integration between 9 and 12 Å and over the entire second peak, 9−15 Å, gives a contribution of 0.11 and 0.20 eV, respectively. The remainder of the total reorganization free energy, 0.55 − 0.11 − 0.20 = 0.24 eV, or 44%, is due to the dielectric response of the solvent that is separated from the cofactor by more than 15 Å. As one can see in Figure 6A, ρ_λ does not approach zero at the edge of the box closest to Ru, d_1

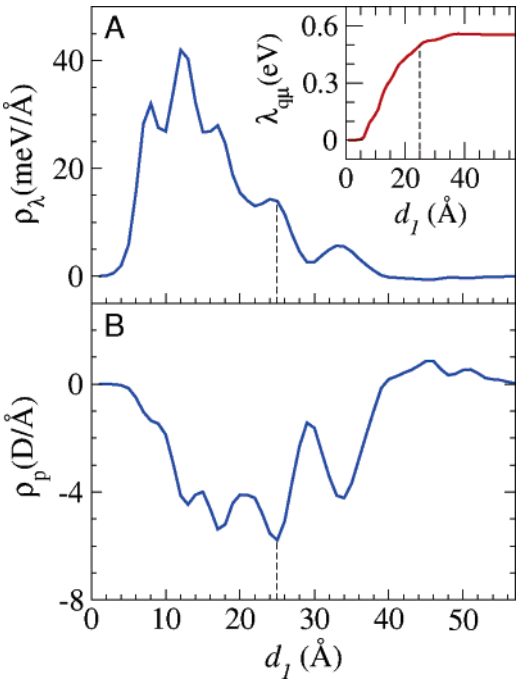

Figure 6. (A) Solvent reorganization free energy density for oxidation of cofactor POR1 (eq 2). $\rho_\lambda(d_1)$ is defined in eq 28 and shown as a function of distance d_1 from the center of mass of ionizable atoms of cofactor POR1. The inset displays the integral of solvent reorganization free energy density, $\lambda_{q\mu}(d_1) = \int_0^{d_1} \mathrm{d}\, d_1' \rho_\lambda(d_1')$, which approaches a plateau value $\lambda_{q\mu}^{\mathrm{wat}} = 552$ meV (see Table 7). (B) Dipole reorientation density, $\rho_p(d_1)$ (eq 29), illustrating dipolar reorientation of the solvent upon oxidation. (Note, the dipole moment of a TIP3P water molecule is 2.35 D.) The densities in panels A and B represent the total reorganization free energy and change of dipolar orientation of all water molecules in a spherical shell of width 1 Å centered at a distance d_1. The densities in panels A and B were smoothed by convolution with a Gaussian of width 1 Å. Dashed lines indicate the distance between Ru and the closest edge of the simulation box.

= 25 Å (dashed line). The density at distances $d_1 > 25$ Å comes from solvent molecules located in the corners of the cubic simulation cell and at the far end of the protein. An increase of box size would certainly lead to an increase of density at distances $d_1 > 25$ Å, showing that the bulk contribution cannot be neglected. Using a continuum approximation, we have estimated this contribution in section 3.5 to be about 0.1 eV.

Self-Exchange. The analysis of outer-sphere reorganization for self-exchange is summarized in Table 6, and the ranking of residues according to reorganization free energy contribution is given in Table 8. Decomposing the energies similarly as for oxidation, we find that slightly less than half of the total outer-sphere reorganization free energy, λ^o, is due to the protein, $\lambda^p = 0.59$ eV (46%). The remainder is solvent reorganization, 0.68 eV (54%). The protein reorganization free energy is twice as high as for oxidation, while the solvent contribution increases by a factor of 1.1 only, giving a total increase of λ^o by a factor of 1.5 relative to oxidation. Note that for *inter*-protein electron transfer, λ^o(self-exchange) = $2\lambda^o$(oxidation) in the limit of infinite separation of donor and acceptor proteins.

The free energy contribution of each residue, λ_r, was calculated from a single run with POR1 in the oxidized state and POR2 in the reduced state (state A = (III,II)). This run yields the average electron-transfer energy, $\langle \Delta E_r \rangle_A$. Owing to the symmetry of the bundle, the average ET energy in the charge-transferred state B, $\langle \Delta E_r \rangle_B$, is given for the first 64 residues by $-\langle \Delta E_{r+64} \rangle_A$, $r = 1,...,64$ (see Figure 1D). Therefore,

Table 8. Ranking of Residues According to the Reorganization Free Energy Contribution λ_r for Electron Self-Exchange between Two RuDPP Cofactors, POR1 and POR2[a]

rank	residue	λ_r (meV)	λ_{qq} (meV)	$\lambda_{q\mu}$ (meV)	charge (e)	$\langle d \rangle_A$ (Å)	$\Delta\langle d \rangle$ (Å)	$\Delta\langle \Delta p^{II} \rangle$ (D)
1	"wat"	742	0	730	0	25.1		−0.01
2	GLN16	68	0	85	0	10.0	0.98	−6.25
3	GLN23	46	0	41	0	7.7	−0.53	0.64
4	LEU33	45	80	−36	1	15.6	4.43	1.19
5	ALA40	37	0	22	0	6.7	0.60	−0.82
6	LYS28	35	10	36	1	13.8	−0.01	−2.72
7	GLU3	31	26	6	−1	18.6	−1.92	−1.10
8	ALA8	30	0	14	0	6.6	0.63	−0.49
9	GLN41	26	0	36	0	8.5	0.08	−1.20
10	POR1	25			−1.850	0.3	0.04	−4.76
11	POR2	25			−2.537	0.3	0.04	−4.76
12	LYS60	22	14	16	1	14.1	−0.37	−1.36
13	HIS22	18	−56	34	0.425	4.8	0.15	−0.41
14	GLN30	17	0	7	0	12.5	−0.53	0.49
15	LYS21	15	5	14	1	11.3	0.09	−1.20
16	ALA4	14	0	11	0	14.8	−2.12	−0.07
17	GLN38	13	0	17	0	13.1	−0.04	−0.24
33	HIS54	3	−29	12	0.425	4.9	−0.07	0.48
68	"ions"	−124	−125	0	8	25.1		

[a] λ_r is decomposed into charge−charge and charge−dipole contributions, λ_{qq} (eq 24) and $\lambda_{q\mu}$ (eq 25), respectively; $\lambda_r \approx \lambda_{qq} + \lambda_{q\mu}$ for large $\langle d \rangle_A$. Charge refers to the total charge of each residue. The average distance between the center of mass of a residue and the center of mass of all ionizable atoms of the nearest cofactor is denoted $\langle d \rangle_A = \langle \min(d_1,d_2) \rangle_A$, and the change of average distance upon electron transfer is $\Delta\langle d \rangle = \langle d \rangle_B - \langle d \rangle_A$. The dipole reorientation upon electron transfer, $\Delta\langle \Delta p^{II} \rangle$, was calculated according to eq 30. "wat" refers to the sum of contributions of all water molecules and "ions" to the sum of contributions of all sodium and chloride ions in the system. The distances for "wat" ("ions") are averaged over all water molecules (ions) in the system, and $\Delta\langle \Delta p^{II} \rangle$ is the average per water molecule. Due to symmetry, only residues with residue number smaller than 64 are listed; see discussion in section 3.6.

$\lambda_r = (\langle \Delta E_r \rangle_A + \langle \Delta E_{r+64} \rangle_A)/2$ and $\lambda_{r+64} = \lambda_r$. In Table 8, only residues with residue numbers smaller than or equal to 64 are listed. With the exception of ALA40 and ALA8, all residues ranked in the top 10 have again dipolar (GLN) or charged (LYS,GLU) side chains or are charged terminal residues (LEU). Highly ranked dipolar residues are close to one of the cofactors, $\langle d \rangle_A = \langle \min(d_1,d_2) \rangle_A \leq 10$ Å, whereas highly ranked charged residues can be separated from the cofactors by more than 18 Å. This is in accord with the short-ranged nature of dipolar interactions and the long-ranged nature of electrostatic interactions. As mentioned previously, the latter are weakly screened in the interior of the bundle.

Dipolar reorganization can be quantified by the change of dipole orientation upon electron transfer,

$$\Delta\langle \Delta p^{II} \rangle = \langle \Delta p^{II} \rangle_B - \langle \Delta p^{II} \rangle_A \tag{30}$$

$$\Delta p^{II} = \vec{\mu}_r \cdot \vec{d}_2/d_2 - \vec{\mu}_r \cdot \vec{d}_1/d_1 \tag{31}$$

Except for GLN23, $\Delta\langle \Delta p^{II} \rangle$ is negative for all dipolar residues ranked in the top 10. The dipolar response is remarkably large for GLN16, −6.25 D, resulting in the highest contribution, with 68 meV. The relatively large contribution of the apolar alanine residues ALA40 and ALA8, 37 and 30 meV, respectively, is likely related to reorganization of backbone atoms and subsequent change of dipole orientation, $\Delta\langle \Delta p^{II} \rangle = -0.8$ and −0.5 D, respectively. The reorganization free energy of the charged residues LEU33 and GLU3 can be understood in terms of repulsion from and attraction to the nearest cofactor that becomes oxidized (POR2)/reduced (POR1) during self-exchange.

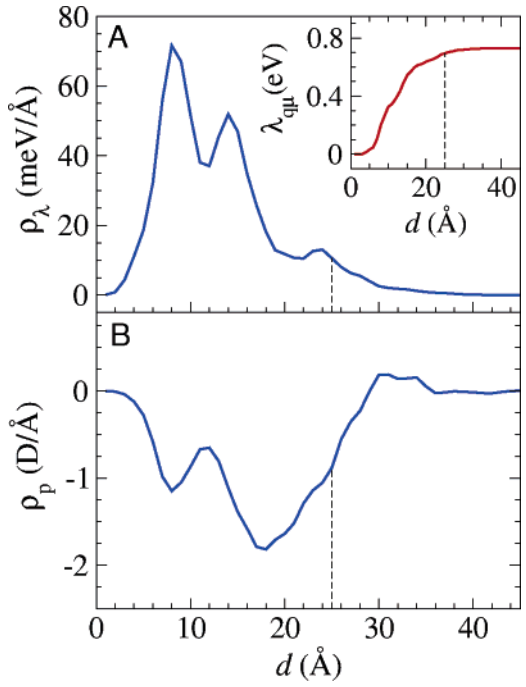

Figure 7. (A) Solvent reorganization free energy density for electron transfer between two cofactors, POR1 and POR2, binding to the four-helix bundle (eq 3). $\rho_\lambda(d)$ is defined in eq 32. The inset displays the integral of solvent reorganization free energy density, $\lambda_{q\mu}(d) = \int_0^d \mathrm{d}\, d' \rho_\lambda(d')$, which approaches a plateau value $\lambda_{q\mu}^{\mathrm{wat}} = 730$ meV (see Table 8). (B) Dipole reorientation density, ρ_p (eq 33), showing dipolar reorganization of the solvent upon electron transfer. The densities in panels A and B represent the total reorganization free energy and change of dipolar orientation of all water molecules in bins of width 1 Å, centered at a distance d. The latter is defined as the shortest distance to either of the cofactors, POR1 or POR2: $d = \min(d_1,d_2)$. The densities in panels A and B were smoothed by convolution with a Gaussian of width 1 Å. Dashed lines indicate the distance between Ru and the closest edge of the simulation box.

The distance between positively charged residue LEU33 and POR2 increases by $\Delta\langle d\rangle = \langle d\rangle_B - \langle d\rangle_A = 4.4$ Å, leading to a reorganization free energy contribution of 45 meV. Conversely, the distance between negatively charged GLU3 and POR2 decreases by −1.9 Å upon oxidation, giving a contribution of 31 meV. However, not all charged residues respond to electron transfer by change of separation distance. The distance between LYS28 and POR1 remains almost unchanged, despite a reorganization free energy contribution of 35 meV. In this case, reorientation of the long, positively charged side chain of LYS28 is the source for reorganization free energy.

We have analyzed the solvent contribution for self-exchange again by means of reorganization free energy density, $\rho_\lambda(d)$ (eq 32), and dipole reorientation density (eq 33), In the case of self-

$$\rho_\lambda(d) = \mathrm{d}\, \lambda_{q\mu}(d)/\mathrm{d}\, d \tag{32}$$

$$\rho_p(d) = \langle \mathrm{d}\, \Delta p^{\parallel}(d)/\mathrm{d}\, d\rangle_B - \langle \mathrm{d}\, \Delta p^{\parallel}(d)/\mathrm{d}\, d\rangle_A \tag{33}$$

exchange, $\lambda_{q\mu}(d)$ and $\Delta p^{\parallel}(d)$ are the reorganization free energy and dipole reorientation of all water molecules that are within a distance d to either of the cofactors, POR1 or POR2 (computed using eqs 25 and 31, respectively). The distribution of ρ_λ shown in Figure 7A exhibits two distinct and broad peaks which correlate well with ρ_p (Figure 7B). The first peak, centered at 8 Å, integrates to 0.38 eV at 12 Å, that is, 52% of the total solvent reorganziation free energy $\lambda_{q\mu}^{\mathrm{wat}} = 0.730$ meV. As discussed earlier for oxidation, this contribution comes from dipolar reorganization and increase (decrease) of the number of water molecules in the vicinity of the cofactor that becomes oxidized (reduced). The second peak, between 12 and 22 Å, is centered at 14 Å and contributes 0.28 eV. The density ρ_λ has a finite value at the nearest box edge (25 Å) but seems to converge faster to zero than for oxidation. The missing reorganization free energy of the bulk solvent was roughly estimated in section 3.5 to be 0.06 eV.

4. Conclusion

Sampling the gap fluctuations for a total of 20 ns, we have obtained a reorganization free energy of 0.90 ± 0.04 eV for oxidation of RuDPP and a reorganization free energy of 1.36 ± 0.08 eV for electron self-exchange between two RuDPP cofactors bound to the four-helix bundle. While inner-sphere contributions are small, about 0.1 eV, outer-sphere contribution accounts for almost the total reorganization free energy. We find that the solvent is the primary outer-sphere medium for oxidation, while the protein contribution is only 31%. The latter increases to 46% for electron self-exchange, making protein and solvent reorganization equally important. Our results are little dependent on the detailed distribution of the excess electron on RuDPP due to the long distance between cofactor and the parts of the outer sphere that contribute most to reorganization. For this reason, we do not expect significant changes if the classical point charges of the cofactor are replaced by the explicit electron density in QM/MM calculations. The effect of explicit treatment of electronic polarization of protein and solvent remains to be investigated, however. Despite the difficulties involved in measuring reorganization free energies, we are confident that our results can be verified with experimental kinetic data in the near future.

As in natural proteins, the structure and dynamics of the nonbiological RuDPP cofactor are virtually inert to oxidation, thereby providing one important requirement for efficient electron transfer. The protein contribution to self-exchange reorganization free energy is relatively small, 0.59 eV, but larger than estimated for cyt c/cyt c, ∼0.4 eV.[22] However, the efficiency of electron transfer in the bundle is drastically reduced by the large solvent reorganization of 0.68 eV, which is much higher than suggested for cyt c/cyt c, 0.1−0.2 eV,[22] and for hemoglobin hybrids.[23] The large solvent reorganization is not due to a few water molecules that temporarily penetrate the bundle nor due to the first solvent shell of the protein but is a consequence of dipolar reorganization of the entire solvent. The solvent reorganization free energy density exhibits a peak at a separation distance 14 Å from the cofactors and decays only slowly to zero, indicating that the change of electric field upon self-exchange is not as effectively screened by the four-helix bundle protein.

Our results indicate that fast electron transfer in the designed four-helix bundle can be achieved if the surrounding medium has a low dielectric constant. This, however, requires that electronic coupling be sufficiently large, which we have not investigated in this work but can be assumed from the relatively short porphyrin edge-to-edge distance of about 9 Å. Returning to an aqueous environment again, we suggest that the reorganziation free energy could be decreased by ∼0.2 eV if the dipolar glutamine residues GLN16 and GLN23 in the vicinity of the cofactors are mutated into less polar amino acids.

The Gaussian nature of gap fluctuations allowed us to use the linear response formalism of electron-transfer theory, making it possible to break down the free energy barrier into contributions from single amino acid residues and solvent. In this way, we have obtained a detailed picture of outer-sphere reorganization, which is one key factor determining the efficiency of electron transport in the bundle. We are confident that the present analysis and future molecular dynamics investigations will provide helpful information for tailoring redox proteins that exhibit optimal electron-transfer properties.

Acknowledgment. We thank Prof. J. Saven for providing the model structure of the four-helix bundle protein and Prof. M. J. Therien, Prof. W. F. DeGrado, and Dr. C. Frey for helpful discussions. J.B. thanks Dr. M. Dal Peraro, Dr. K. Spiegel, and Dr. A. Kohlmeyer for valuable advice on QM/MM and classical molecular dynamics simulations. The Pittsburgh Supercomputing Center is acknowledged for providing computer time on a CRAY XT3. Less computer-intensive calculations were carried out on a local cluster at the LRSM, University of Pennsylvania. NIH is acknowledged for financial support.

Supporting Information Available: Force field parameters for RuDPP; system parameters for QM/MM simulations and classical MD simulations; results of test calculations for monovalent pseudopotentials and of convergence calculations for cutoff radius r_{NN}; complete ref 39; atomic charges used in the simulations; two figures showing rmsd and gap fluctuations. This material is available free of charge via the Internet at http://pubs.acs.org.

JA063852T